Master Thesis

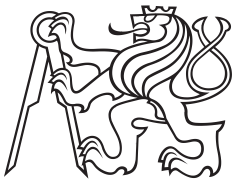

Czech Technical University in Prague

F3

Faculty of Electrical Engineering
Department of Microelectronics

Harmonic Transponder with RF Identification Capability

Giorgi Aptsiauri

Supervisor: doc. Ing. Milan Polívka, Ph.D.
Field of study: Electronics and Communications
Subfield: Electronics
May 2023

Acknowledgements

I would like to thank my supervisor Dr. Milan Polívka for his professional insight and guidance throughout all stages of this thesis. I would also like to thank Dr. Milan Švanda for his help with sample preparation.

Declaration

I declare that this work is all my own work and I have cited all sources I have used in the bibliography.

Prague, 25. May 2023

Abstract

In this work, the concept of a harmonic transponder based on triple-band UHF patch antenna loaded with a Schottky diode with RF identification capability operating at f_1, $f_2 = 2f_1$, and $f_3 = f_2 + \Delta f$ frequencies is demonstrated. A frequency shift coding technique is used to create a unique identifier, which is defined by the spacing between the received power peaks at frequencies f_2 and f_3. Additional f_3 resonance is achieved using capacitive coupling mechanism by introducing a pair of passive strips gap-coupled to the antenna patch. Proof-of-concept samples were made, measured and the results were compared with the simulation. The best conversion loss of 4.68 dB has been obtained at f_2 for one of the samples and two distinguishable peaks were observed in the received signal power. The ability of the proposed RFID-enabled harmonic transponder to encode eight data identifiers via frequency shift coding has been demonstrated in simulation.

Keywords: Antennas, capacitive coupling, frequency conversion, harmonic transponders, impedance matching, nonlinear load, patch antenna, RFID, Schottky diode

Supervisor: doc. Ing. Milan Polívka, Ph.D.
Room: A4-108,
Technická 1902/2,
Praha

Abstrakt

V této práci je navržen koncept harmonického transpondéru využívající třípásmovou patch anténu se Schottkyho diodou se schopností RF identifikace pracující na frekvencích f_1, $f_2 = 2f_1$, a $f_3 = f_2 + \Delta f$. K vytvoření unikátního identifikátoru, který je definován vzdáleností mezi maximy přijímaného výkonu na frekvencích f_2 a f_3, se používá technika kódování frekvenčním posunem. Dodatečná rezonance f_3 je vybuzena pomocí dvojice pasivních pásků kapacitně vázaných mezerou k anténnímu patchi. Byly vyrobeny zkušební vzorky, provedena měření a výsledky porovnány se simulací. Nejlepší konverzní ztráta 4.68 dB byla dosažena u jednoho ze vzorků na frekvenci f_2 a měřením byly zjištěny dva rozlišitelné vrcholy v přijímaném signálu. Schopnost navrhovaného harmonického transpondéru zakódovat osm datových RFID identifikátorů pomocí kódování s frekvenčním posunem byla prokázána simulací.

Klíčová slova: Anténa, flíčková anténa, frekvenční konverze, harmonický transpondér, kapacitní vazba, impedanční přizpůsobení, nelineární zátěž, RFID, Schottky dioda

Překlad názvu: Harmonický transpondér se schopností RF identifikace

Contents

Figures

Tables

MASTER‘S THESIS ASSIGNMENT

I. Personal and study details

Student's name: **Aptsiauri Giorgi** Personal ID number: **510872**

Faculty / Institute: **Faculty of Electrical Engineering**

Department / Institute: **Department of Microelectronics**

Study program: **Electronics and Communications**

Specialisation: **Electronics**

II. Master’s thesis details

Master’s thesis title in English:

Harmonic Transponder with RF Identification Capability

Master’s thesis title in Czech:

Harmonický transpondér s možností RF identifikace

Guidelines:

Integrate the RF identification functionality into the harmonic transponder [1] using one or two passive strip resonators by frequency shift coding (FSC) method [2, 3]. Create one or two additional resonances in the vicinity of the second harmonic frequency using capacitive coupling between the strip resonator(s) and the outer arms of the harmonic transponder.
Create an EM simulation model and geometrically tune the structure so that the input impedance at all three (four) operating frequencies is complex conjugate to the load diode impedance.
Demonstrate the creation of an identification code by the FSC method by frequency detuning the passive resonator(s).
Fabricate a sample of the transponder and verify its parameters by measurement.

Bibliography / sources:

[1] M. Polivka, V. Hubata-Vacek and M. Svanda, 'Harmonic Balance/Full-Wave Analysis of Wearable Harmonic Transponder for IoT Applications,' in IEEE Transactions on Antennas and Propagation, vol. 70, no. 2, pp. 977-987, Feb. 2022.
[2] X A. Vena, E. Perret, and S. Tedjini, 'High-Capacity Chipless RFID Tag Insensitive to the Polarization,' IEEE Transactions on Antennas and Propagation, vol. 60, no. 10, pp. 4509-4515, Oct 2012.
[3] M. Polivka, M. Svanda, High Encoding Capacity Chipless RFIDTag, European conference on Antennas and Propagation (EuCAP), 2023, accepted

Name and workplace of master’s thesis supervisor:

doc. Ing. Milan Polívka, Ph.D. Department of Electromagnetic Field FEE

Name and workplace of second master’s thesis supervisor or consultant:

Date of master’s thesis assignment: **02.02.2023** Deadline for master's thesis submission: _____

Assignment valid until: **22.09.2024**

doc. Ing. Milan Polívka, Ph.D. Supervisor’s signature	prof. Ing. Pavel Hazdra, CSc. Head of department’s signature	prof. Mgr. Petr Páta, Ph.D. Dean’s signature

III. Assignment receipt

The student acknowledges that the master’s thesis is an individual work. The student must produce his thesis without the assistance of others, with the exception of provided consultations. Within the master’s thesis, the author must state the names of consultants and include a list of references.

Date of assignment receipt	Student’s signature

0.1 List of Acronyms

HT Harmonic Transponder 3

FSC Frequency Shift Coding vi

RCS Radar Cross Section 8

RFID Radio Frequency Identification vi

ID Identification 22

REGCOMA Radiating Edges Gap-Coupled Microstrip Antenna . . . 6

RSL Received Signal Level 5

HR Harmonic Radar 3

RF Radio Frequency 12

VNA Vector Network Analyzer 35

LPF Low Pass Filter 35

FSL Free Space Loss 34

EIRP Equivalent Isotropically Radiated Power 42

IC Integrated Circuit vii

CL Conversion Loss 12

Chapter 1

Basic Concepts

Wireless sensing, tracking, and identification are attracting more and more attention due to the proliferation of portable wearable electronic devices. The miniaturization of electronic devices through large-scale integration on single-die silicon chips has made portable devices inexpensive and widely available to the general population. Many industries, such as agriculture, logistics, healthcare, transportation, automotive, etc., rely heavily on digital technologies. A major part of some industries is tracking and identification of targets such as parcels, livestock, patients, cars, etc. [7]. This widespread digitization has necessitated the improvement of wireless sensing and identification technology and, as a result, numerous papers have been published on the topic of wireless identification [8].

The most widely used identification mechanism in industry today is RFID technology[9]. In RFID technology, an active or passive transponder, also called a *tag*, consisting of an antenna and a chip, is interrogated by a *reader* at a specific frequency (uplink). An RFID tag then responds at the same or a different frequency. The chip typically contains identification information that is communicated to the reader via a downlink connection[7].

Another approach is often called a Harmonic Radar (HR), shown in Fig. 1.1. In this approach, a target, also known as a Harmonic Transponder (HT), typically composed of a dual-band antenna loaded by a nonlinear element such as diode, is illuminated at the fundamental frequency f_1, and the response is transmitted back at an integer multiple of f_1, that is, at a harmonic of f_1. Any harmonic multiple can be used, but practical implementations typically use the second harmonic because out of all harmonics, the highest level of

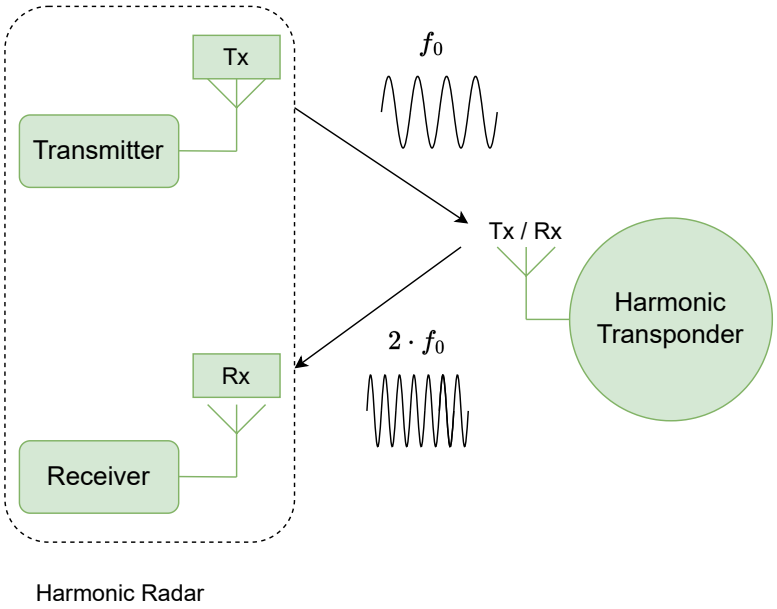

Figure 1.1: Operating principle of a harmonic radar.

power is concentrated in the second one ($2f_1$) [9].

A radar based on the harmonic principle has an advantage in complex environments. If a tag communicated back at the same frequency it was illuminated by, reflections from the surrounding environment could distort the signal. This issue is mitigated by harmonic radar where it is clear that the signal at $2f_1$ is reflected by the tag and not the surroundings. The principle works because objects in nature do not exhibit non-linear properties at powers used in modern-day wireless communication systems [10, 11].

The principle of harmonic radar was first introduced in a 1968 paper and later studied as an anti-collision system for automobiles[12]. It has also been used to detect rebar corrosion[13]. A number of studies have also attempted to track insects with a harmonic transponder, using a lightweight antenna directly matched to a Schottky diode[14, 15, 16, 17]. For insect tracking applications, harmonic transponders have a significant advantage over conventional radars because the harmonic response allows unambiguous signal identification in a complex environment [9].

There are two main types of harmonic transponders. One type is where the impedance of an antenna is directly matched to the diode's at the operating frequencies. The second type is where external matching circuits are used for matching. Both types have been extensively studied in previous works [10].

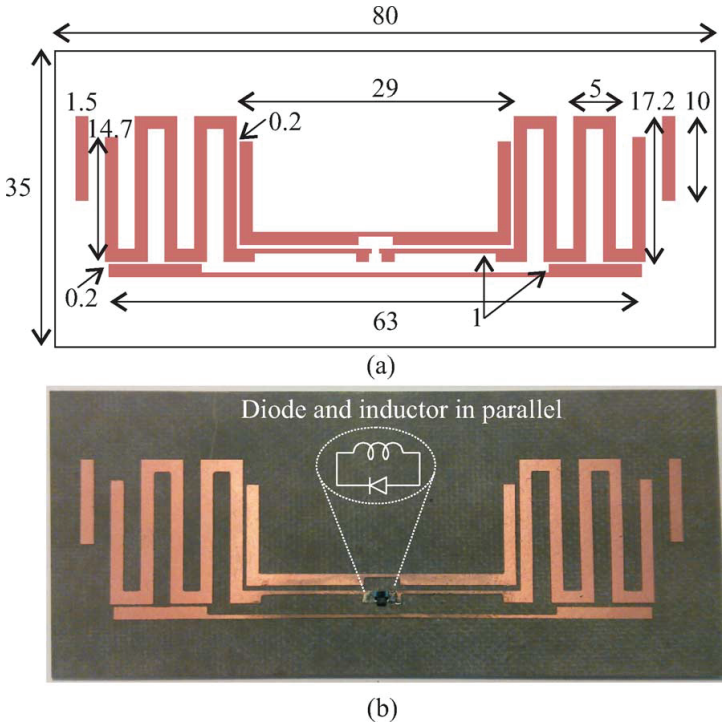

Figure 1.2: Transponder tag design from [1]. (a) Dimensions of the designed tag. (b) A photograph of the harmonic transponder.

A significant amount of work has been done in characterizing harmonic transponders via circuit simulators and analytical approaches [9, 10, 5]. Also, numerous works have demonstrated harmonic transponders at different frequencies - mostly noncompliant with current spectrum allocations, therefore for demonstration purposes only. One such design is shown in Fig. 1.2, operating at $f_1 = 1\,\text{GHz}$ and $2f_1 = 2\,\text{GHz}$ where the diode and the antenna are directly matched. The measured Received Signal Level (RSL) of the given transponder at the second harmonic versus the fundamental tone is shown in Fig. 1.3. Since the impedance of the diode is directly matched to that of the antenna's at two harmonically separated frequencies, $f_1 = 1\,\text{GHz}$ and $2f_1 = 2\,\text{GHz}$, therefore, the received power in the downlink peaks only at $2f_1$.

In this work, we aim to achieve similar results as in Fig. 1.3, except that an additional peak is created in the power response due to capacitive coupling near the second harmonic in the RSL. By varying the frequency of the additional peak, data identifier can be introduced onto a tag. To this end, we attempt to add a pair of passive elements to create additional resonances closely spaced to the second harmonic signal that exploit Frequency Shift Coding (FSC) technique to create a unique identifier (ID) of the harmonic transponder [5]. The coupling mechanism used in this concept is capacitive, since the passive strips are gap-coupled.

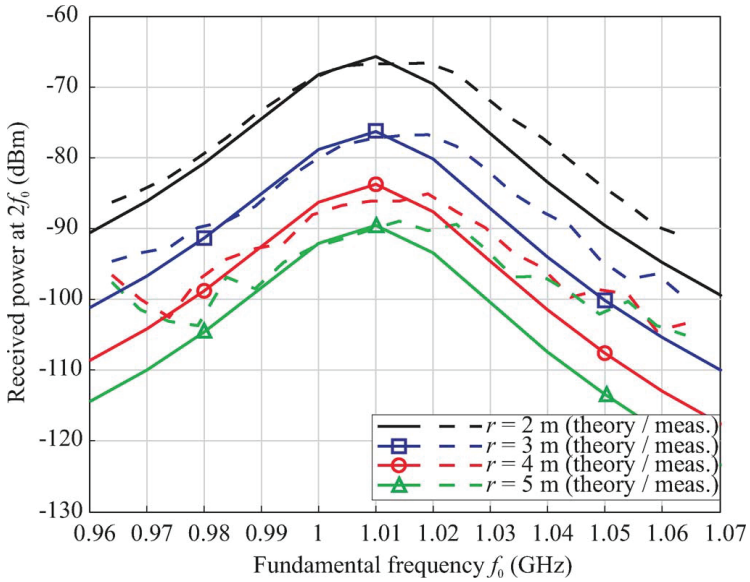

Figure 1.3: Harmonic response of the transponder shown in Fig. 1.2.

1.1 Capacitive Coupling

The concept of capacitive coupling is well known in electronics. The most common application for a coupling capacitor is where it is necessary to block the DC current but allow the AC current to pass, such as in amplifiers where the DC and AC currents must be isolated. In the field of antenna design, capacitive coupling was introduced by Gupta in 1981 [18, 2]. In this work, a classical rectangular patch antenna is designed with additional parasitic patches as shown in Fig. 1.4. The structure was named Radiating Edges Gap-Coupled Microstrip Antenna (REGCOMA), referring to the coupling mechanism being a gap, rather than direct coupling. The purpose of this work was to improve the inherently narrow bandwidth of a classical rectangular patch antenna.

The principle of operation is based on the idea of resonance superposition. In this technique, parasitic patches placed on the same substrate near the radiating patch are designed so that their resonance frequencies are close to those of the radiating patch [2]. An illustrative example is shown in Fig. 1.5, where the superposition of two resonances leads to an improved, wider bandwidth.

In this work, we will use the concept of capacitive coupling, i.e., coupling of the radiating element to parasitic ones, in order to create new resonances

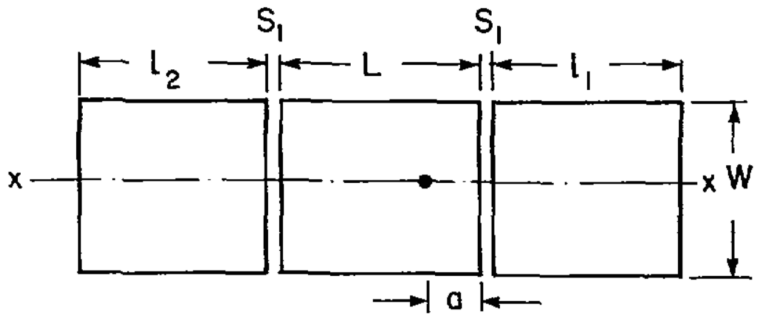

Figure 1.4: Radiating edges gap-coupled microstrip patch antenna (REGCOMA). The patch in the middle is excited at distance a from its edge. And, two parasitic patches are placed next to the excited patch.

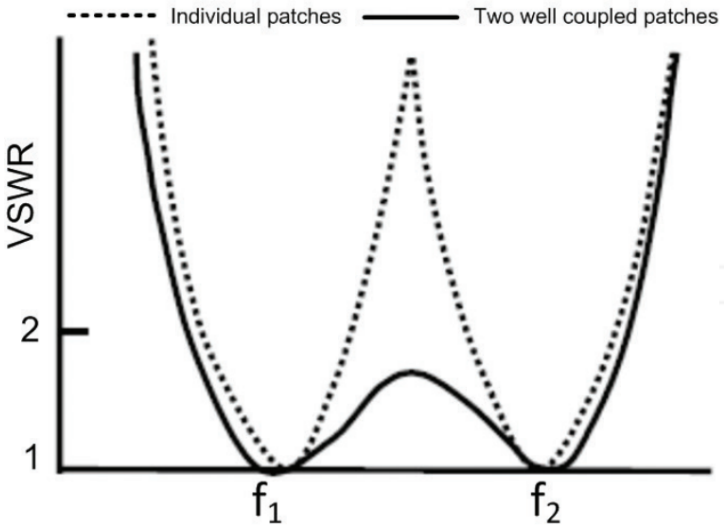

Figure 1.5: Superposition of closely spaced resonances lead to bandwidth enhancement achieved with parasitic patches [2].

closely spaced but separated from the second harmonic tone in the antenna S11 characteristics. A Schottky diode is then connected to the antenna, matched at three frequencies that would provide a harmonic response to the reader when illuminated with a fundamental tone. In addition, by varying the width of the gap, we can adjust the effect of the coupling, thereby slightly changing the frequency of the third harmonic tone, f_3. The ability to change the resonant frequency by changing only one antenna parameter is a key enabling factor for the concept of merged HT-RFID tag presented in this thesis. This idea is explored in the next section.

1.2 Frequency Shift Coding

The principle of FSC has been used before in chipless RFID tags [19, 20]. The application of this technique to the design of chipless RFID tags helps to improve its figures of merit, as follows

$$\textbf{Spectral capacity (bits/GHz)} = \frac{\textbf{(number of bits)}}{\boldsymbol{BW}\ \textbf{[GHz]}} \tag{1.1}$$

$$\textbf{Spatial density (bits/cm}^2\textbf{)} = \frac{\textbf{(number of bits)}}{\boldsymbol{size}\ \textbf{[cm}^2\textbf{]}} \tag{1.2}$$

$$\textbf{Encoding capacity}\left(\frac{\textbf{bits}}{\lambda^2 \times \textbf{GHz}}\right) = \frac{\textbf{(number of bits)}}{\boldsymbol{size}\ (\lambda^2) \times \boldsymbol{BW}\ \textbf{[GHz]}} \tag{1.3}$$

As it can be seen from all three expressions ((1.1), (1.2), (1.3)) the left hand side of the expressions is directly proportional to the *(number of bits)*. The value of *(number of bits)* can be increased by the FSC technique, to pack more data into a chipless RFID tag, hence its importance.

The principle of FSC is that instead of using the presence/absence of a coding element [3], a parameter of the coding element (e.g. a physical dimension) can be modified to change its Radar Cross Section (RCS), thereby shifting the resonant frequency. This principle is demonstrated in Fig. 1.6 [4]. in Fig. 1.6.a, presence/absence coding method is used where bits *1011* are encoded in a way that

(a) bit *1* is represented by the presence of a strip - thereby causing the respective resonant peak to appear in the RCS response.

(b) bit *0* is represented by the absence of a strip - thereby causing the respective resonant peak *not* appear in the RCS response.

It can be seen that, the presence/absensce coding, in this example, requires four $\lambda/2$ coding elements.

An alternative method to encode the same data using FSC technique is demonstrated in Fig. 1.6.b. Using the FSC technique, the same bits *1011* are encoded in a way that

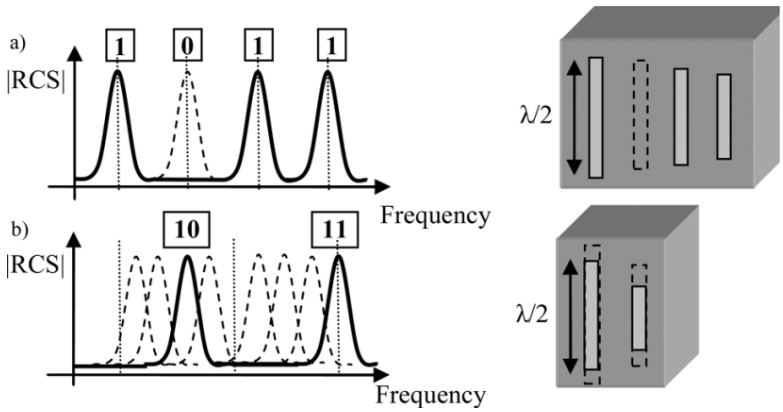

Figure 1.6: a) Prescence/absence coding technique introduced by Jalaly [3]. b) frequency shift coding technique [4].

(a) bits *10* are represented by only one $\lambda/2$ element. In this case, the four combinations (*00, 01, 10, 11*) are obtained by varying the length of this coding element.

(b) bits *11* are also represented by only one $\lambda/2$ element. The only difference is that the initial length is smaller (i.e., higher resonance peak), and slight variations in length lead to resonances in the neighborhood of the initial RCS response peak.

From the illustrative example in Fig. 1.6, it can be seen that the FSC technique can significantly increase the encoding capacity of chipless RFID systems (see (1.3)).

We also use the FSC technique in this thesis, but the metric of the RFID tag we want to measure is the harmonic response generated by the nonlinear element instead of RCS. Also, we intend to vary the resonant frequencies f_2 and f_3 by varying the capacitive coupling (i.e., varying the gap) between the patch antenna and the passive strips placed next to it on the same substrate.

1.3 On the Nature of Nonlinearities

It is well known in radio electronics that every nonlinear system produces harmonics of the fundamental frequency [21]. This phenomenon can be either intended, e.g. in mixers, frequency multipliers or undesired, e.g. in power amplifiers. In the case of RF mixers, nonlinearity is the phenomenon that enables its functionality. In its basic form, a diode can be used as a passive

mixer whose operation is solely dependent on the nonlinearity of a diode [21]. On the other hand, we desire to have perfectly linear amplifiers whose output amplitude is a scalar multiple of the input, therefore, free from harmonics. In our case, nonlinearity is a desired effect, since it allows the conversion of power from the fundamental tone to the second harmonic.

To showcase this phenomenon, let us model a nonlinear system approximated by a third order polynomial as

$$y(t) = \alpha_1 x(t) + \alpha_2 x^2(t) + \alpha_3 x^3(t) \tag{1.4}$$

where all terms are a function of time. If a sinusoid of the form $x(t) = A\cos(\omega t)$ is applied to the nonlinear system characterized by (1.4), then

$$\begin{aligned} y(t) &= \alpha_1 A\cos(\omega t) + \alpha_2 A^2\cos^2(\omega t) + \alpha_3 A^3\cos^3(\omega t) \\ &= \alpha_1 A\cos(\omega t) + \frac{\alpha_2 A^2}{2}(1+\cos(2\omega t) + \frac{\alpha_3 A^3}{4}(3\cos(\omega t) + \cos(3\omega t)) \\ &= \frac{\alpha_2 A^2}{2} + \left(\alpha_1 A + \frac{3\alpha_3 A^3}{4}\right)\cos(\omega t) + \frac{\alpha_2 A^2}{2}\cos(2\omega t) + \frac{\alpha_3 A^3}{4}\cos(3\omega t) \end{aligned} \tag{1.5}$$

In (1.5), the first term is the DC resulting from the second-order nonlinearity. The second term is the fundamental. The third and fourth terms are the second and third harmonics, respectively. From the expression, we can see that when a sinusoidal input is applied to a nonlinear system, higher-order frequency components appear at the output. A similar principle is used in the harmonic transponder, where a Schottky diode represents a non-linear system in this analogy, producing higher order harmonics when excited with a sinusoidal input.

1.4 Proposed Concept of an HT with RF Identification Capability

This work focuses on adding RFID functionality to a harmonic transponder presented in [5]. To this end, we have attempted to demonstrate that capacitive coupling of passive strips to the radiating patch can lead to additional resonance peaks. Variable frequency peaks of f_2 and f_3 harmonic tones by varying the gap between the strips and the patch will be used to demonstrate data identifier implementation using the FSC technique.

Chapter 2

Design and Simulation of RFID Antenna

A harmonic transponder is nothing more than an antenna and a nonlinear device, e.g., a diode [1]. The input impedance of the antenna is matched to that of the diode at two harmonically separated frequencies, f_1 and $2f_1$. Harmonic transponders have an advantage over regular RFID technology at single frequencies in a sense that the signal at $2f_1$ clearly identifies the presence of a harmonic transponder in an environment with parasitic reflections. The disadvantage of a harmonic transponder is that only the presence of the tag can be identified. In this work, we intend to introduce the concept of FSC (Section 1.2) to the design of harmonic transponders in order to encode data identifier onto it.

2.1 RFID Tag Antenna

In this section the simulated design of the RFID transponder tag along with FSC demonstration is presented. A dual-band patch antenna used as a basis in this work was originally designed in a diploma thesis for a harmonic transponder [22, 5]. In a later publication, the same antenna principle was used to design a harmonic transponder shown in Fig. 2.1, along with theoretical insight into the design [5]. In this work, an HSMS-2820 Schottky diode was selected for the design because of its low Conversion Loss (CL) at the frequency of interest and slightly higher real part of the impedance, which is useful for impedance matching. Fig. 2.1c shows the plots of the antenna and diode impedances. It can be seen that matching is achieved at 0.867 GHz and 1.734 GHz (note that the complex conjugate of the diode impedance is plotted). In this thesis, we have used the same diode because it simplifies antenna modification, as the impedance of the existing design provides a useful starting point for matching to the complex impedance of the diode. In addition, radiation patterns and other antenna parameters have already been reported in [5].

To introduce an additional resonance, a pair of passive strips was placed symmetrically next to the patch along the resonant dimension. The model of the antenna, with a 50 Ω port for simulation, is shown in Fig. 2.2. RO4350B commercial Radio Frequency (RF)/microwave substrate was used with $\epsilon_r = 3.48$, and metallization thickness of 55 µm. We can see from Fig. 2.2b, that (almost) ideal matching is achieved by optimizing at three frequencies simultaneously, namely, 0.867 GHz, 1.7089 GHz, and 1.7614 GHz. It can also be seen that by adding the two passive strips shown in Fig. 2.2a (top and bottom, gap is 1 mm), an additional third resonance has appeared in the impedance plot. Dashed vertical pink lines show the matching frequencies. Final dimensions of the designed antenna are shown in Fig. 2.3. Since impedance matching requires consideration of both the antenna and the diode, discussion of this topic is deferred to the next section.

It is also important to look at the S11 parameters when matching two RF devices. As described in Section 2.2, to correctly interpret the S11 parameters of an RFID antenna, we must normalize the antenna impedance to the frequency-dependent complex impedance of the diode. The normalization can be done with the following expression

$$\frac{Z_D(f) - Z^*_{ant}(f)}{Z_D(f) + Z^*_{ant}(f)} \tag{2.1}$$

With this principle in mind, Fig. 2.4a shows a correct S11 plot of the antenna in Fig. 2.2a. The matching frequencies are clearly marked by dashed vertical pink lines and are the same as those shown on the impedance plot in Fig. 2.2b. More details on impedance matching are given in the next section. It is worth noting that there is another dip in the S11 plot at about 1.92 GHz. This can be explained by looking at the antenna and diode impedance plot in Fig. 2.2b, where we can see that at or after about 1.9 GHz, the match becomes good, leading to the dip in S11. Since we need to demonstrate the tag's ability to encode data by frequency shifting, we also show the S11 when the gap between the passive strips and the patch is increased to 2 mm in Fig. 2.4b - with unchanged patch dimensions. Using the effect of capacitive coupling, by changing only one parameter (gap, therefore capacitance) on the antenna substrate, data identifier can be introduced on the tag, thereby realizing the desired FSC technique.

In the same way as above, we show the transmission coefficient τ, which is computed as follows,

$$|\tau|_{\mathrm{dB}} = 10 \log \left(1 - \left(\left| \frac{Z_{ant} - Z11_D^*}{Z_{ant} + Z11_D} \right| \right)^2 \right) \tag{2.2}$$

and shown in Fig. 2.5 along with simulated combined τ, later explained and presented in Section 3.3 together with measured values. Here, we note that the significance of the the combined τ is that it allows us to rapidly estimate the power peaks in the received signal for a harmonic transponder [23]. Since the matching of both the real and imaginary parts of the impedance is almost perfect (Fig.2.2b) in simulation, we observe ideal (0 dB) transmission at the design frequencies as well. The ideal transmission will not hold in the next chapter, where we will perform the measurements on the given RFID tag design. This is due to mismatches in the true (measured) impedances of the antenna and the diode, resulting in mismatch losses. Also note that due to the narrow-band nature of the transmission coefficient τ at f_1 (see in Fig. 2.5a), deterioration of transmission is already predicted by the simulated combined τ metric.

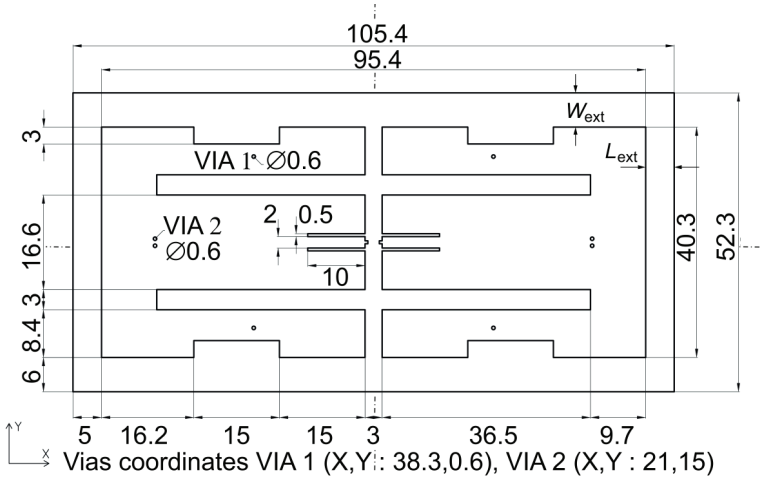

(a) : Dimensions of the antenna and via positions.

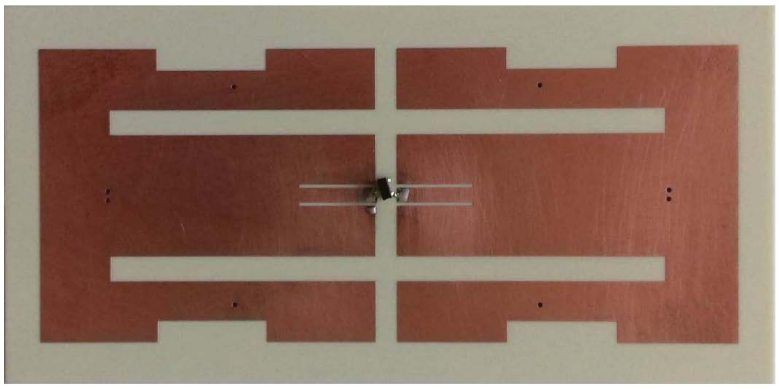

(b) : A photograph of a fabricated antenna and a connected diode.

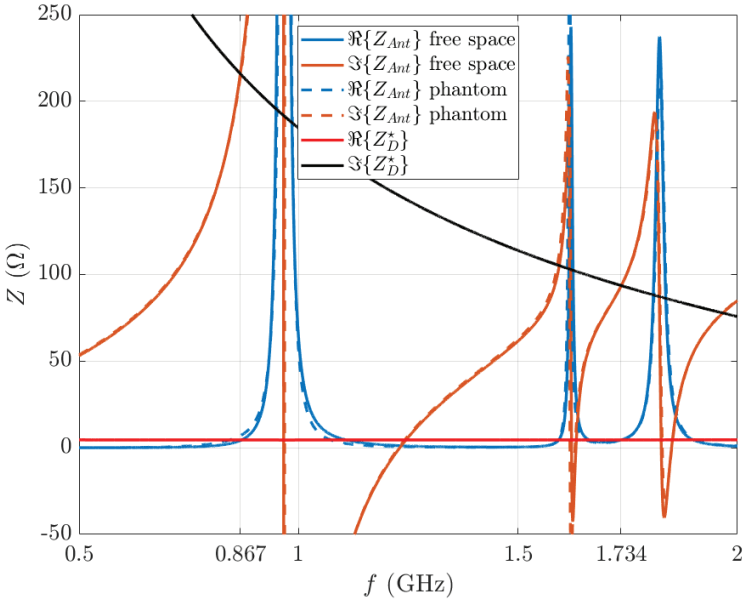

(c) : Impedance characteristics [5].

Figure 2.1: A harmonic transponder design taken from [5].

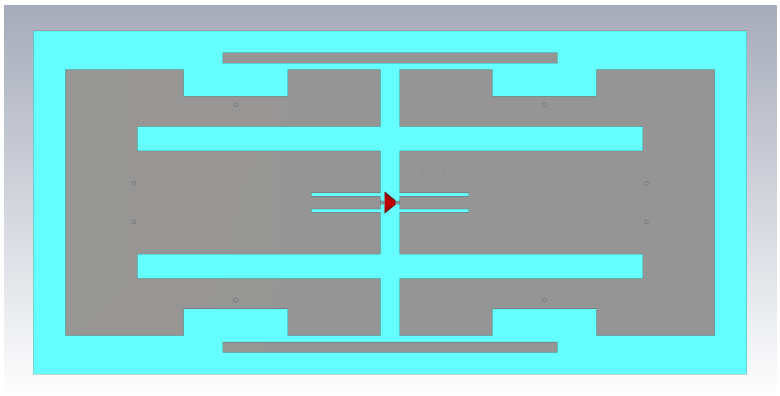

(a):

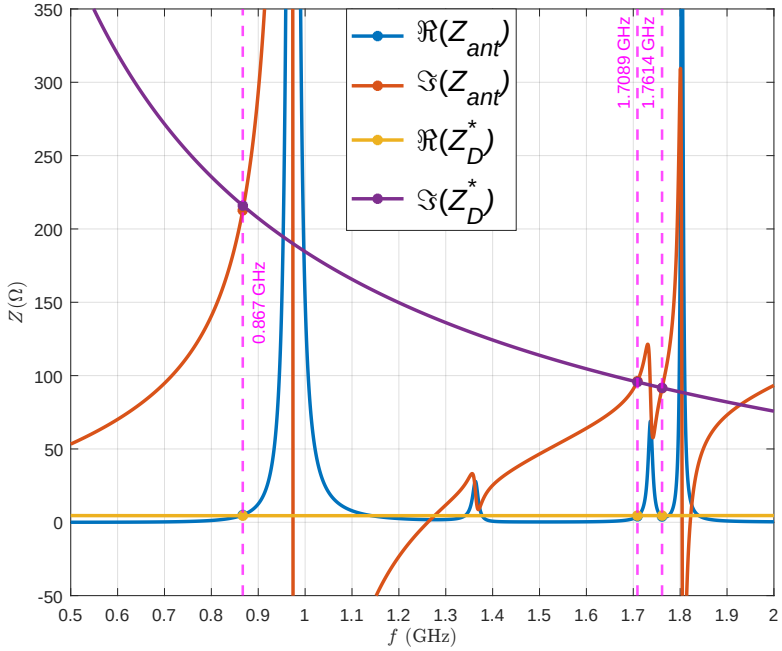

(b):

Figure 2.2: A RFID antenna with passive strips and impedance plots. (a) Top view of the model of the patch antenna for RFID with passive strips added. The gap between the passive strips and the antenna patch is 1 mm. (b) Impedance of the antenna and the diode. The diode's impedance is plotted as conjugate to visualize the matching.

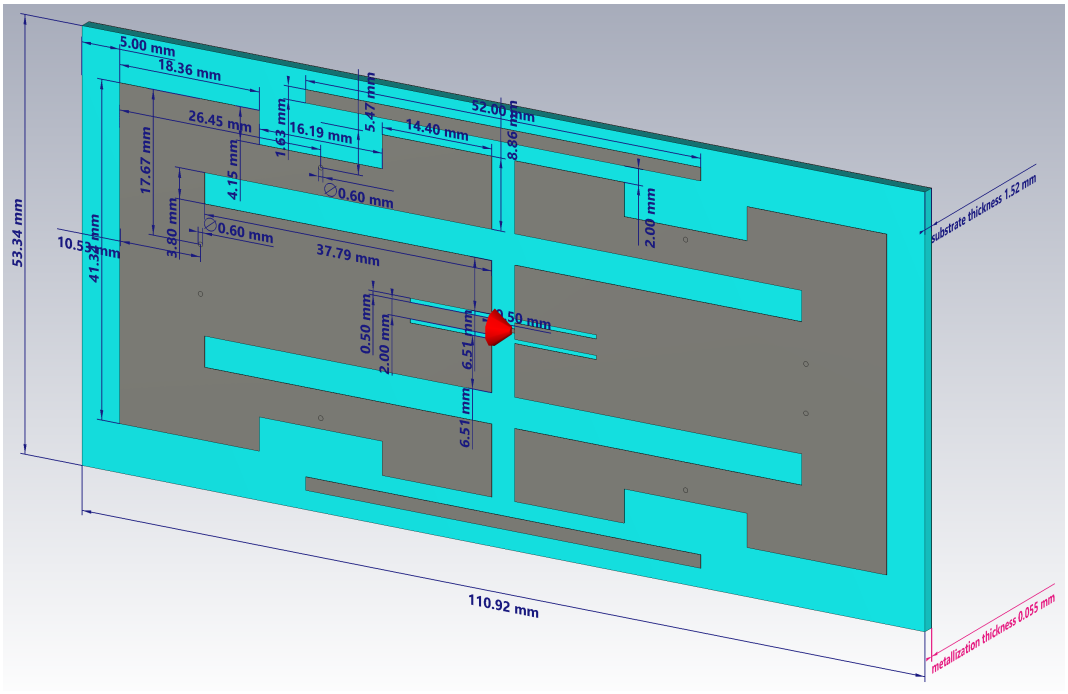

(a):

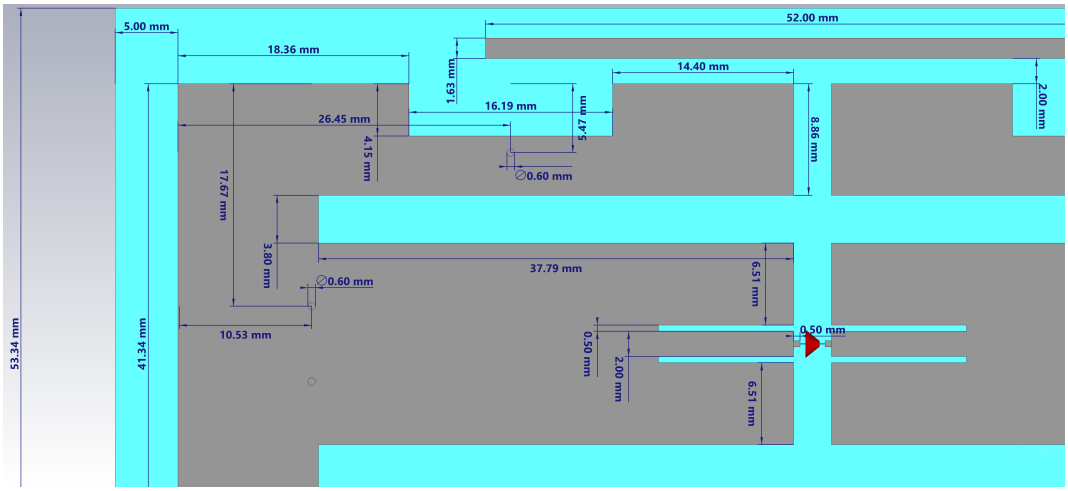

(b):

Figure 2.3: Dimensions of the antenna with passive strips. (a) Full perspective view. (b) Zoomed in on only one quadrant.

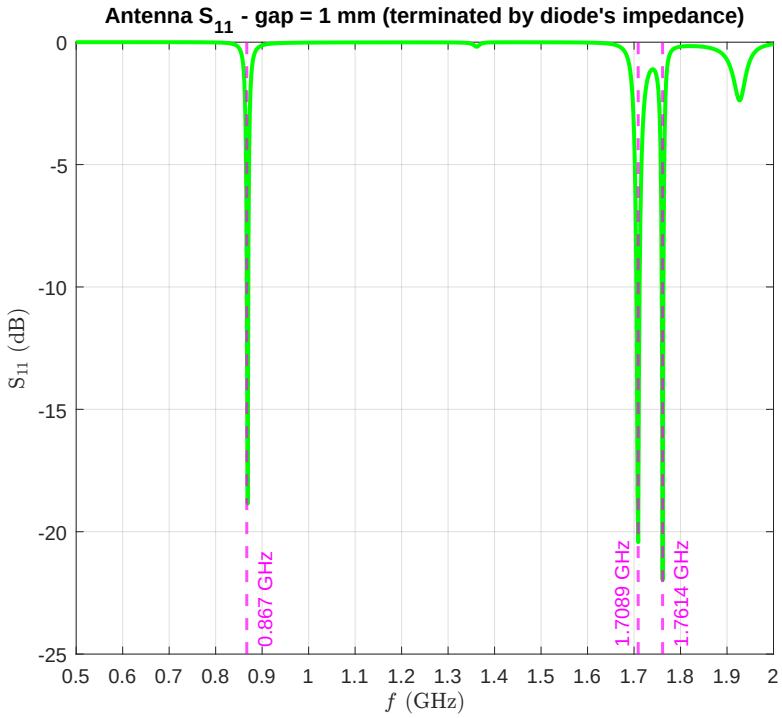

(a):

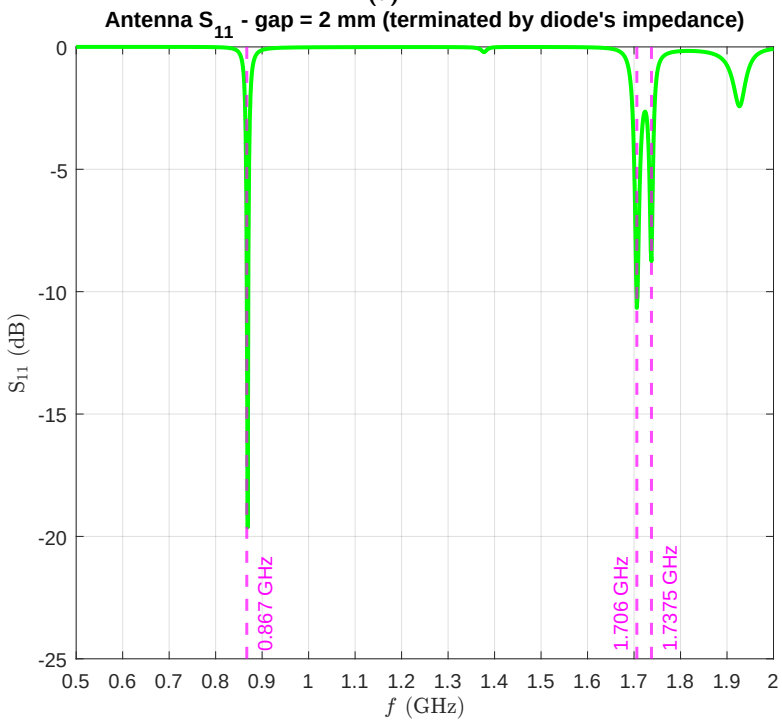

(b):

Figure 2.4: Simulated magnitude of the antenna S11 parameter with its impedance normalized to the diode's frequency-dependent complex impedance. Gap between the antenna patch and the passive strips is (a) 1 mm and (b) 2 mm.

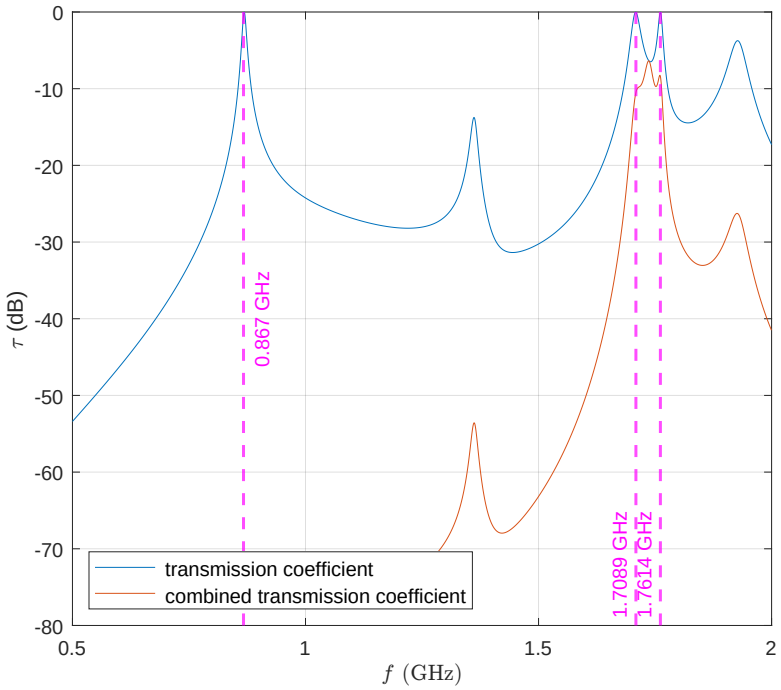

(a):

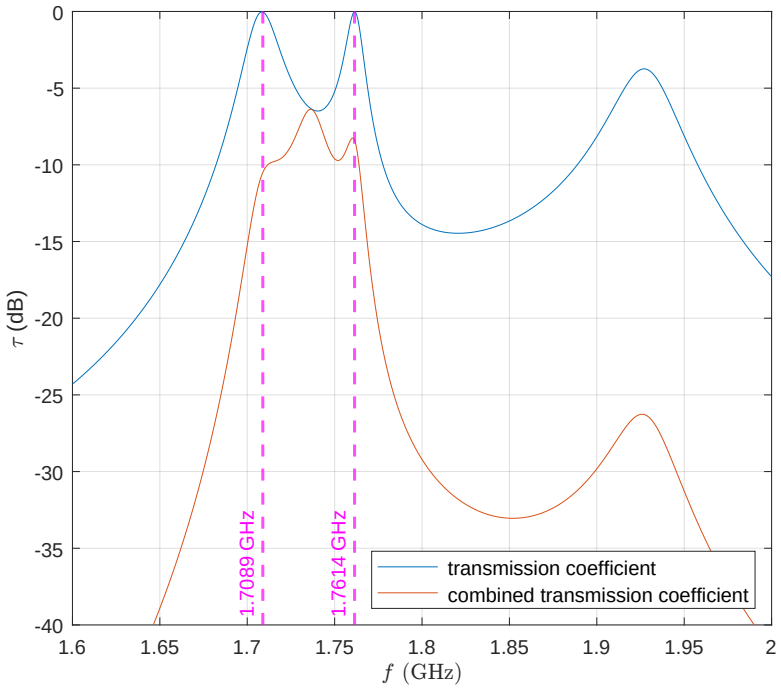

(b):

Figure 2.5: Transmission coefficient τ in the entire band and combined in a way that lower band (0.5 - 1 GHz) is superimposed on the higher band (1.5 - 2 GHz). (a) Entire band. (b) Zoomed in on the peaks.

2.2 Impedance Matching

Impedance matching is one of the most challenging aspects of harmonic transponder design. It is even more challenging for our design because the matching must occur at three frequencies simultaneously. Unlike single-frequency impedance matching for classic RFID tags, a harmonic transponder requires matching at two harmonically separated frequencies, such as $f_1 = 0.867$ GHz and $2f_1 = 1.734$ GHz. Therefore, it is essential to use optimization algorithms available in commercial tools to arrive at the desired antenna impedance.

To proceed with the impedance matching between the antenna and the diode, the impedance of the diode must be obtained. Then the complex impedance of the diode at $f_1 = 0.867$ GHz and the higher band are used for optimization. The impedance of the HSMS-2820 diode was extracted using the free SPICE simulator LTSpice. See Appendix A for a detailed description of the diode impedance extraction method in LTSpice. The impedance of the HSMS-2820 diode is shown in Fig 2.6. The impedance values at the frequencies of interest are given in Table 2.1. It can be seen from both the figure and the table that the real part of the diode's impedance is almost constant over the entire operational band, while the imaginary part changes significantly.

Once the data in Table 2.1 is obtained, the impedance matching optimization can be set up in the commercial antenna simulator CST Studio. However, we must remember that we are not designing a classical harmonic transponder, but one that is capable of coding data using the FSC technique as described in section 1.2. To achieve this, we need to provide additional resonances in the upper band. As shown in section 2.1, additional passive strips were added to the existing antenna to introduce another resonance in the upper band, near $2f_1 = 1.734$ GHz. For RFID purposes, this additional resonance can be used to implement data identifier. The principle is based on the FSC technique, where the parameters (e.g., length, width, or both) of the passive strips can be changed to shift the resonant frequency of only one or both peaks.

Before fabricating the samples, antenna dimensions were optimized for best impedance matching with the diode (with the gap of 1 mm between the patch and the passive strips). For optimization variables, patch dimensions and only the width of the passive strips were used. The goal function was set up to equal complex impedance of the diode at three frequencies 0.867 GHz, 1.712 GHz, and 1.76 GHz where the real and imaginary parts of the complex

frequency (GHz)	Z_D (Ω)
$f_1 = 0.867$	$4.52 - j215.96$
$2f_1 = 1.734$	$4.55 - j93.71$
$f_2 = 1.7089$	$4.55 - j95.65$
$f_3 = 1.7614$	$4.55 - j91.64$

Table 2.1: HSMS-2820 diode impedance values at the frequencies of interest.

impedance were assigned the weights of 10 and 1, respectively. The two given frequencies in the upper band were chosen such that $2 \cdot 0.867$ GHz would be in between them and halves of the frequencies would be close enough to 0.867 GHz to ensure transmission coefficient (τ) no worse than 10 dB lower than the peak at the excitation frequency. In the first step of optimization, particle swarm algorithm was used with the global search options. After global optimization, the antenna dimensions were further optimized with trust regeion framework algorithm with the local search option.

It should be noted that when evaluating the S11 parameters of an antenna intended to be connected to a non-50 Ω load, such as a diode, the S11 parameters must be normalized to the frequency-dependent complex impedance of the load (e.g., a diode) in order to give an accurate representation of its performance. Typically, this is not an issue for classical RF/microwave systems where antennas are designed to match 50 Ω impedance (without reactive part). However, it is of significant importance to us since some full-wave simulators such as CST Studio only allow the user to select a single real excitation port resistance. In our case, we only need to consider the antenna S11 parameter when it is normalized to the frequency-dependent complex impedance of the diode. The normalization is easily done in the *Schematic* tool of CST Studio for evaluating the S11 parameters, where it is possible to select the frequency-dependent complex impedance for the termination port from a file (in our case, the Z11 parameters of the diode). To demonstrate the effect of different termination impedances on the S11 plot, see Fig 2.7. The dashed line shows a typical 50 Ω impedance. The other two curves, blue and green, show the S11 parameters of the antenna when normalized to the impedance of the diode at f_1 and $2f_1$, respectively. Note that in the given S11 comparison, the antenna impedance is already matched to the diode's impedance at the frequencies of interest. It can be clearly seen that accurate results are obtained at and near the impedance to which the S11 parameters are normalized. For this reason, we use the frequency-dependent complex impedance of the diode as the normalization factor for evaluating the S11 parameters.

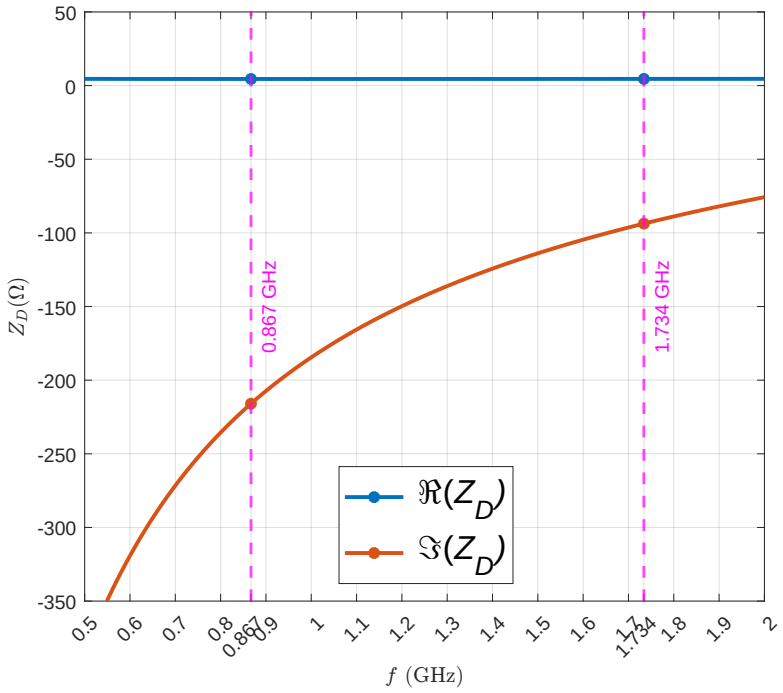

Figure 2.6: The simulated impedance of diode HSMS-2820.

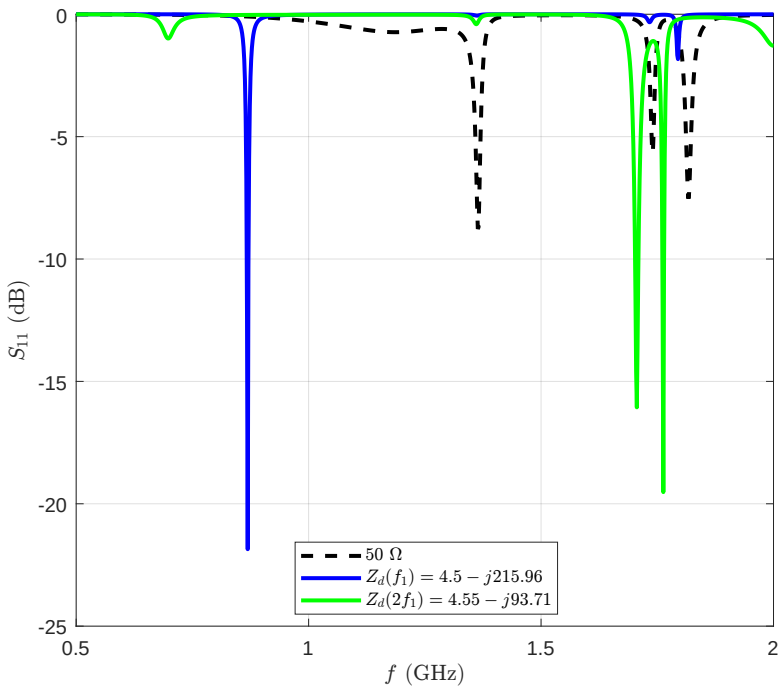

Figure 2.7: The figure shows S11 parameters of the antenna under different termination impedances. Blue and green show S11 when the diode's impedance at f_1 and $2f_1$ are used, respectively.

2.3 FSC on the Transponder

Since the antenna with passive strips has been designed for best matching at three frequencies, next we demonstrate the FSC technique to implement a unique Identification (ID). As described in Section 1.2, unique ID can be implemented using the FSC technique by varying one of the parameters in the design to introduce a predicted frequency shift into the response. Through experimentation, it was found that varying the gap between the passive strips and the patch by about tenths of a millimeter resulted in average frequency shifts of about 2.5 MHz with acceptable distinguishability. The results are shown in Fig. 2.8a over the entire band from 0.5 GHz to 2 GHz, and zoomed in on the span of interest where the frequency shift occurs in Fig. 2.8b. We must note that the S11 parameters presented here are computed when the antenna's simulated impedance is terminated by the diode's frequency-dependent complex impedance.

From the presented simulations, we can make two key observations: (a) impedance matching at f_1 is insensitive to gap variation, and (b) impedance matching is almost insensitive at $2f_1$ as well, effectively allowing us to have fixed frequency of reference to which data identifying frequency shift can be coded. Also note that in all eight cases presented in Fig. 2.8b, dips in S11 magnitude are well below 10 dB mark.

The FSC technique was also attempted by varying the length of the passive strips shown in Fig. 2.9. The dips in S11 at $2f_1 + \Delta f$ are shifted in a desirable manner, however around $2f_1$, there is significant detuning compared to varying the gap shown in Fig. 2.8b. In both cases, by varying the gap or the length, the impedance matching at f_1 hardly changes.

Finally, based on the results presented in this section, varying the gap is preferred because the peak at $2f_1$ remains fixed, while the peak at $2f_1 + \Delta f$ varies predictably with gap.

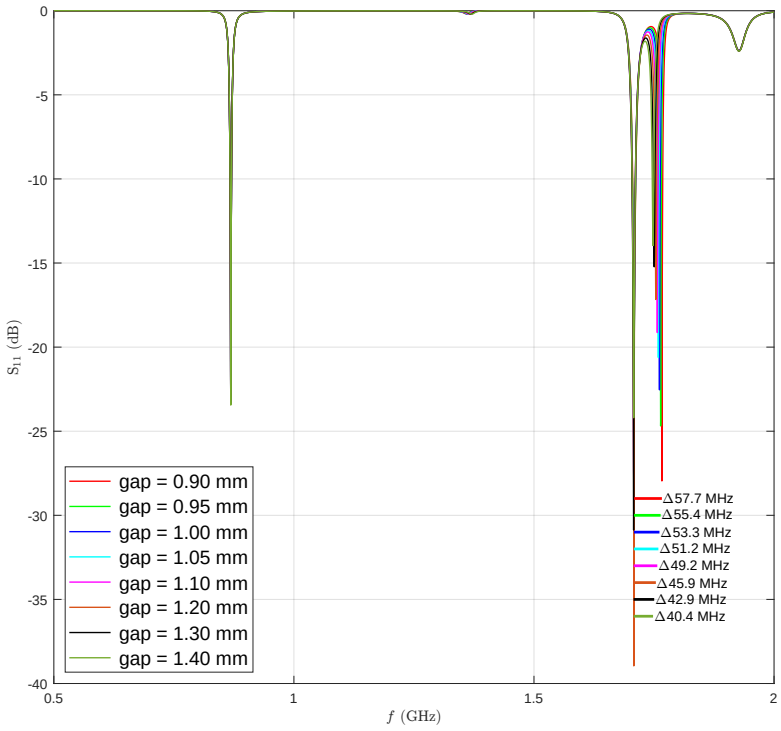

(a):

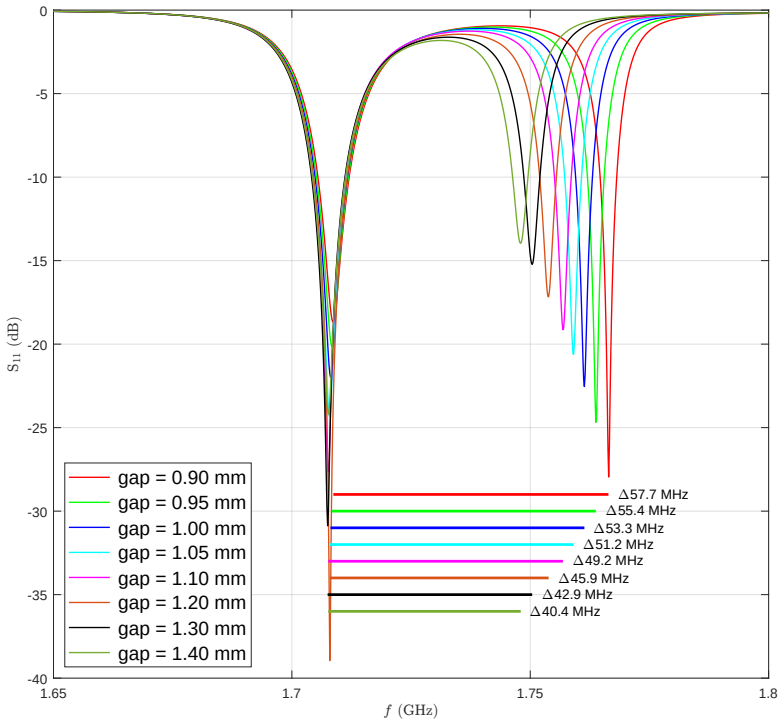

(b):

Figure 2.8: Demonstration of frequency shift coding on the simulated S11 parameters of the RFID-enabled harmonic transponder by varying the gap between the passive strips and the patch. (a) Entire band. (b) Zoomed in on the higher band, where the FSC technique is applied.

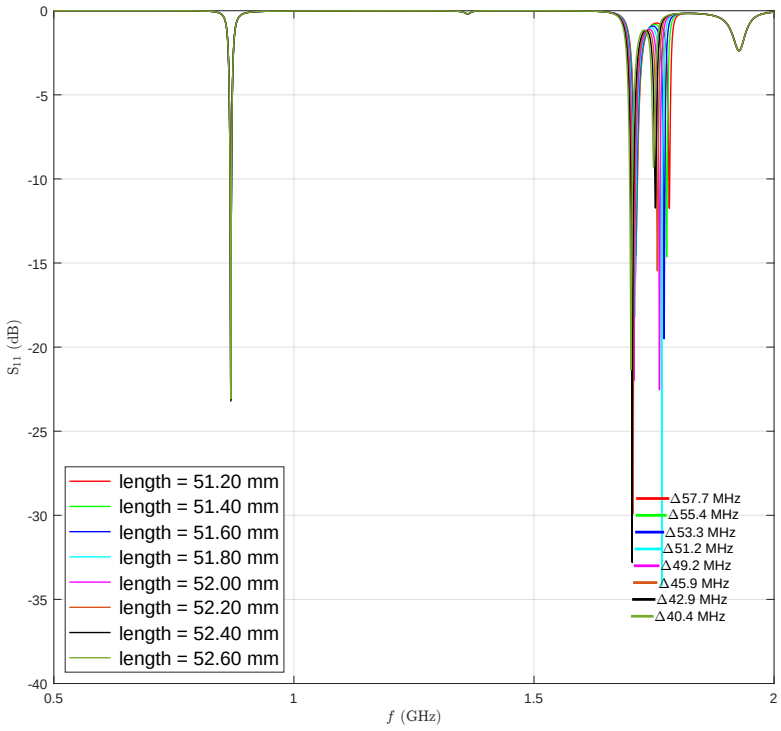

(a):

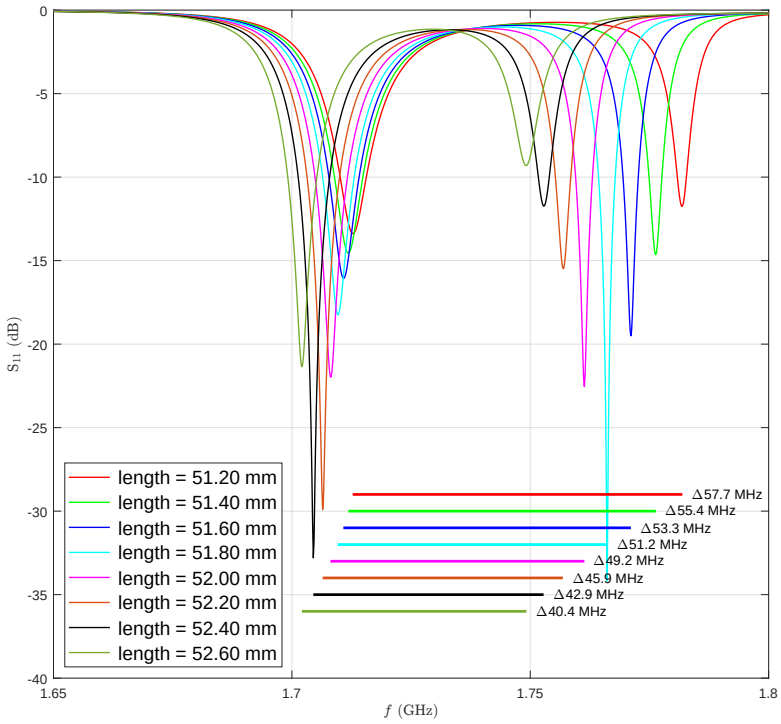

(b):

Figure 2.9: Demonstration of frequency shift coding on the simulated S11 parameters of the RFID-enabled harmonic transponder by varying the length of the passive strips. (a) Entire band. (b) Zoomed in on the higher band, where the FSC technique is applied.

Chapter 3

Measurements

To verify the design developed in Chapter 2, experiments were performed. For these experiments, we used high-end microwave equipment and an anechoic chamber for verifying the concept of capacitive coupling for FSC and testing the parameters of the RFID-enabled harmonic transponder. Table 3.1 shows the equipment used for testing.

3.1 Capacitive Coupling Experiment

One of the earliest experiments for this project was verification of the capacitive coupling mechanism for its potential use in frequency shift coding technique. In other words, we attempted to show that by adding parasitic elements to a single-frequency narrow-band patch antenna, we could introduce additional resonances. As mentioned in Section 1.1, the first accounts of the use of capacitive coupling was for the purpose of bandwidth extension in 1981, by Gupta [18]. In those early works, it was shown that with careful tuning of the parasitic patches, placed next to the radiating one, it was possible to have two resonances (dips in S11 terms) so close that the overlap of the two would superimpose to form one wider band of operation (refer to Fig. 1.5 for an illustrative example).

The experiment was performed using an existing dual-polarized patch antenna which was modelled in CST Studio for the purpose of validation of the coupling concept for FSC. The patch antenna is shown in Fig. 3.1. It

Lab equipment	Purpose
Agilent E5071C (8.5 GHz Network Analyzer)	Measuring antenna impedance
Agilent 85052C 3.5mm Calibration Kit	Calibrating Agilent E5071C
R&S ZVA 40 VNA (10 MHz - 40 GHz)	Tx and Rx for illuminating the HT
ZHL-4W-422+ Power Amplifier	Used in Tx chain for illuminating the HT
VLF-1000+ LPF	Suppressing amplifier's harmonics in Tx chain
RFSPIN QRH11 (Red)	Tx antenna
RFSPIN QRH11 (Gold)	Rx antenna
Attenuator	For power sweep in Tx chain

Table 3.1: Equipment used for measurements and their purpose.

consists of a 47×47 mm rectangular patch with metallization thickness of t =35 µm on a substrate of thickness H =1.5 mm and $\epsilon_r = 3.11$. Coaxial feeding line is exactly 17 mm away from the edge of the metallic patch. The coax feed line is made to be of impedance 50 Ω, shown in Fig. 3.1c. In the same figure, the red indicates the feeding port (only one is excited for our needs).

For the experiment, copper foil tape was used placed right next to the antenna on the substrate. The antenna is shown in Fig. 3.3. The passive strips of length 52 mm, width 1 mm, and 4 mm gap from the patch are placed along the radiating edges in a symmetrical fashion. It can be seen in Fig. 3.2 that by placing the passive strips, the original resonance has shifted slightly (to the left) and a new resonating frequency has appeared close to it. In fact, if we attempted to get the new resonance closer to the existing one, we could enhance the bandwidth of the rectangular patch antenna, but that is not our goal. Our goal is to introduce additional resonances which then can be used for the FSC technique.

This experiment demonstrated that by introducing passive "parasitic" strips to a rectangular patch antenna, additional peaks are indeed introduced. Next, we vary the effect of capacitive coupling by varying the distance of the strips to the antenna. A parametric simulation was performed in CST Studio to demonstrate data encoding principle. The results of varying gap are shown in Fig. 3.4. This demonstration shows that with this antenna, we could implement the data identifier by varying the gap between the strips and the patch. However, with the given antenna and, it would only be possible to transmit encoded information. In other words, since no nonlinearity is integrated on the patch, it would not be able to re-transmit data once illuminated. Naturally, the next step is to integrate a nonlinear device such as a diode into a dual-band (finally, triple-band) patch antenna with passive strips to enable an RFID tag functionality onto it.

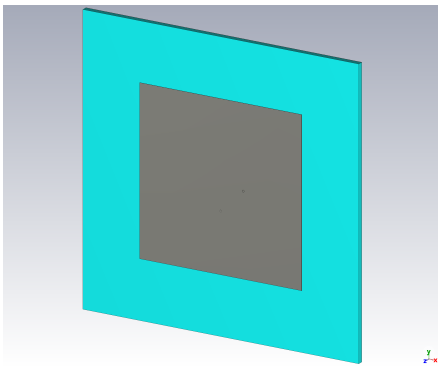

(a) : A patch without passive strips.

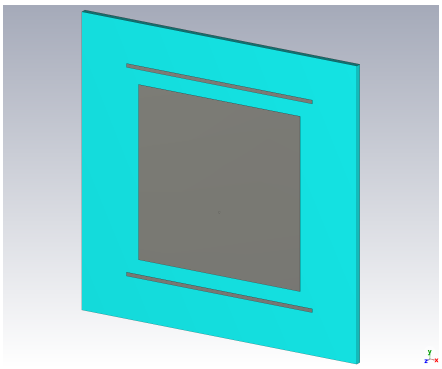

(b) : A patch with passive strips.

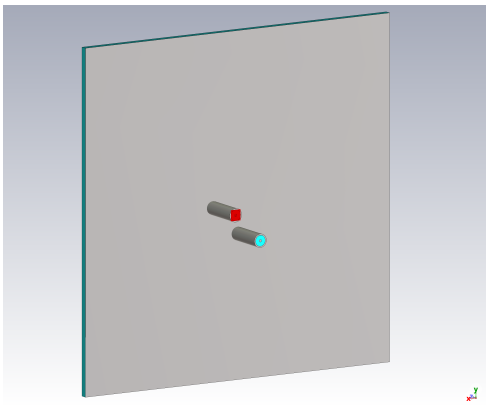

(c) : Back view of the patch antenna. The antenna is excited only at one port (red).

Figure 3.1: A dual-polarized microstrip patch antenna with 50 Ω feeding.

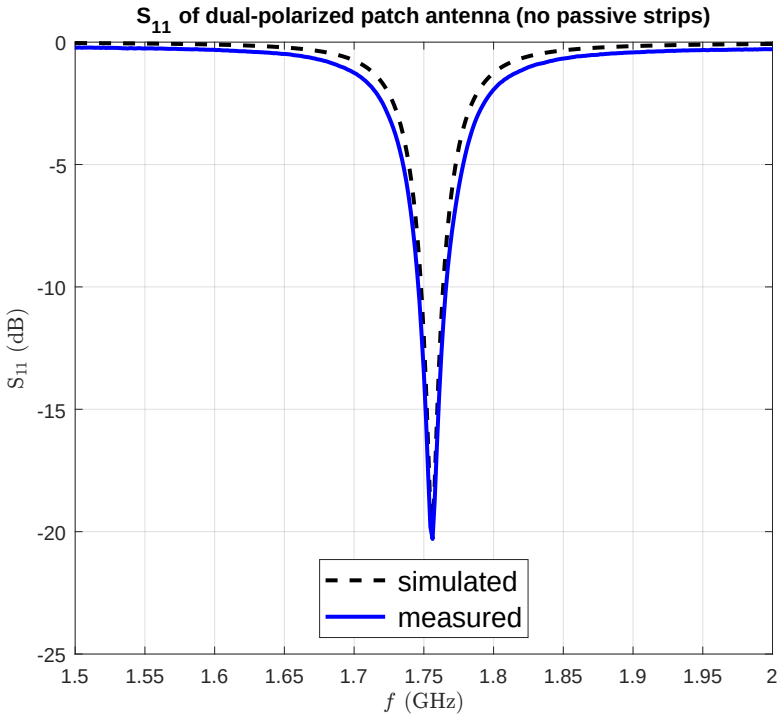

(a):

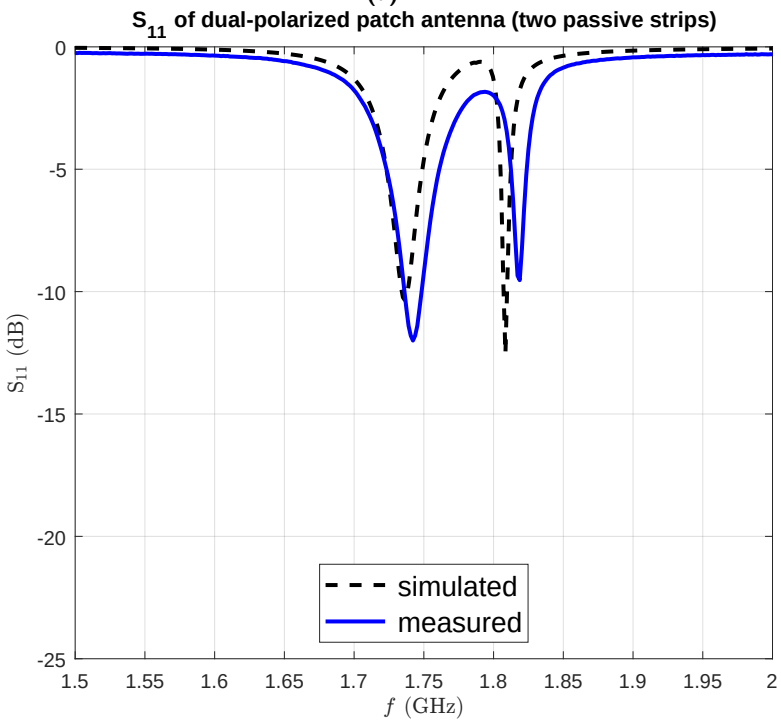

(b):

Figure 3.2: Simulated and measured S11 response of the patch antenna with 50 Ω feeding (a) with no passive strips for the design depicted in Fig. 3.1a, and (b) with passive strips for the design depicted in Fig. 3.1b.

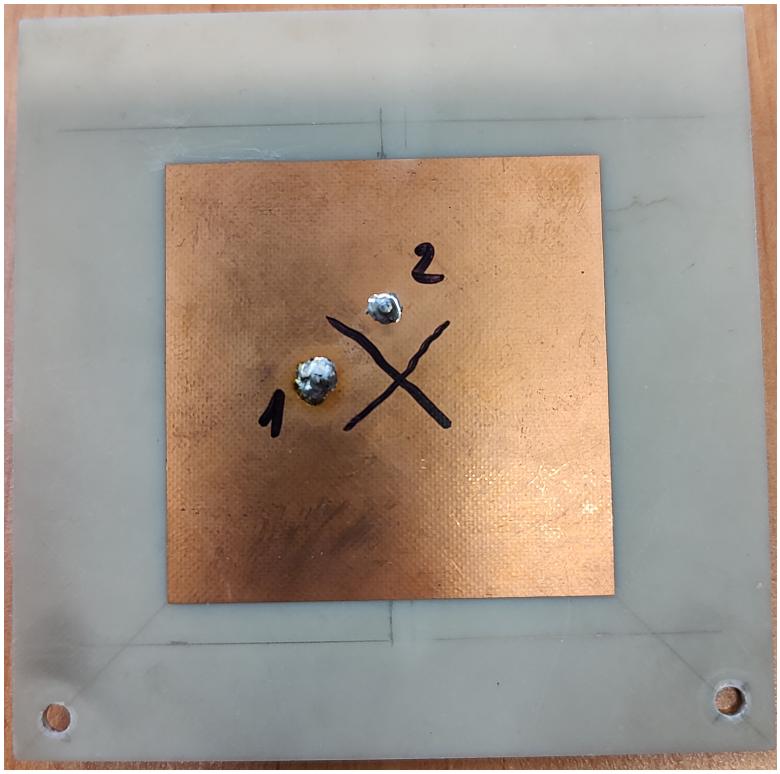

Figure 3.3: Dual-feed patch antenna.

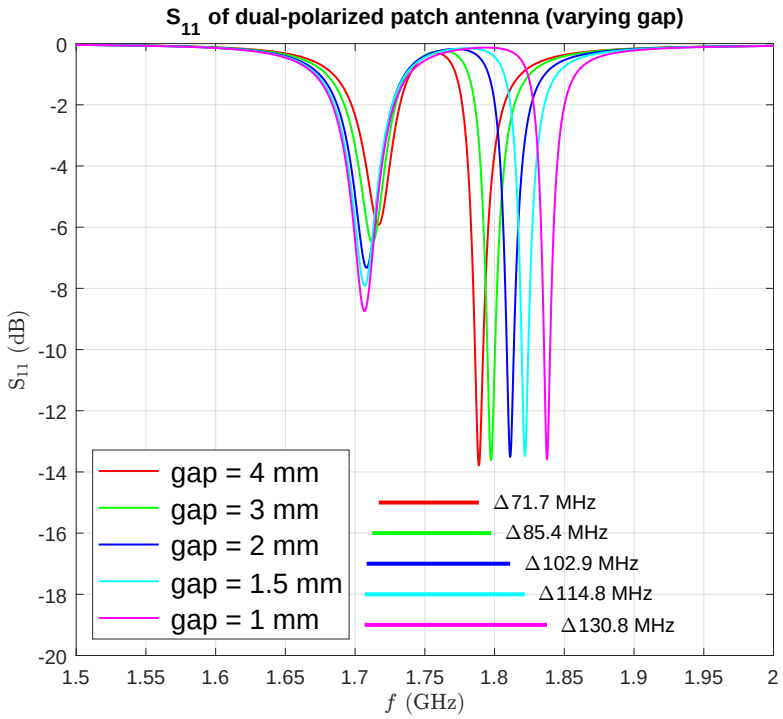

Figure 3.4: Simulated S11 of the patch antenna with different gaps of the passive strips. Gap distance is applied simultaneously to both passive strips. The length and the width of the passive strips are 52 mm and 2 mm, respectively.

Figure 3.5: Measurement of antenna impedance. On the left: a differential probe from [6] is used. On the right: measurement is seen on a Smith chart. Note that a glitch is causing erroneous 180° phase shift which is later corrected in MATLAB.

3.2 Antenna Impedance Measurement

In order to compare the simulated results from the design phase of Chapter 2, and to gain further insight into the real-world operation of the designed RFID tag, the impedance of the antenna was measured. The antenna impedance was measured both in free space and when attached to a human muscle phantom representing an arm. A technique of differential antenna impedance measurement from [6] was used and the following calculation was carried out

$$Z_{diff} = \frac{2Z_0(1 - S_{11}^2 + S_{21}^2 - 2S_{12})}{(1 - S_{11})^2 - S_{21}^2} \tag{3.1}$$

Also, power transmission coefficient between the measured antenna and simulated diode impedances is evaluated with (2.2).

The antenna impedance measurement setup is shown in Fig. 3.5 using a differential probe (from [6]) and a network analyzer (Agilent E5071C) calibrated with the Agilent 85052C calibration kit. The measurement results are presented in the following section.

3.3 Transmission Coefficient

The transmission coefficient along with the measured antenna impedance is shown in Fig. 3.6 and Fig. 3.7 for the two fabricated samples. The total tau, $\tau_{combined}$, first introduced in [23] is also presented, which is calculated by superimposing the transmission coefficient data (Fig. 3.6b and Fig. 3.7b) of $1-2$ GHz on $0.5-1$ GHz (more details in the attached code). Since the presented concept relies on the nonlinearity of the diode to generate the second harmonic, the power transfer from the antenna to the diode is intuitively critical. One way to characterize how well power is transferred is to evaluate the transmission coefficient at the antenna-diode interface, as we have done (Fig. 3.6b and Fig. 3.7b). The second component to consider is how well the diode transfers power back to the antenna (at twice the excitation frequency). To combine the overall effect of transmission, both in the lower band and in the higher band, the combined τ is plotted, which is simply a linear superposition of the transmission coefficients over the same number of data samples in both frequency intervals.

In the figures, we also show with a dashed curve how the performance of the antenna is when it is attached to the human muscle phantom. It can be seen that the peaks are only slightly detuned, which would not affect the operation of the RFID tag.

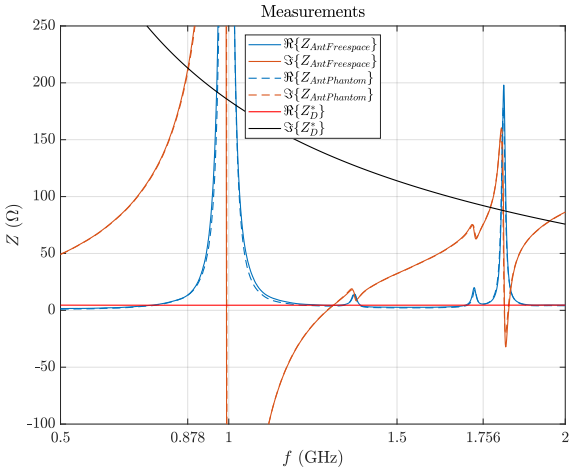

(a) : Measured antenna and simulated diode impedances.

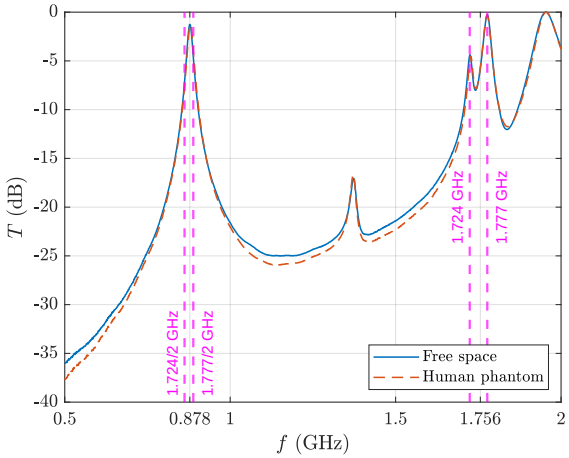

(b) : Transmission coefficient computed with (2.2).

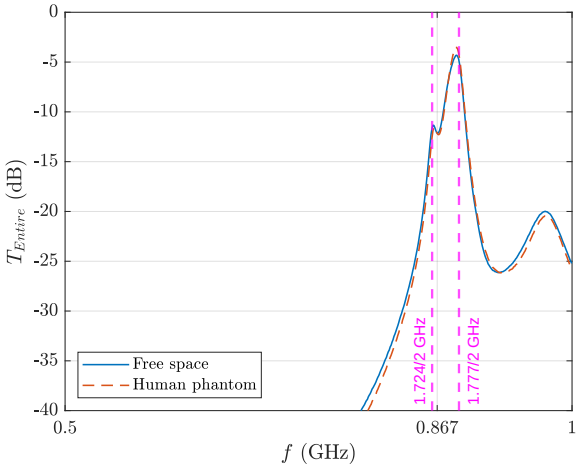

(c) : Combined transmission coefficient τ, computed from the data of Fig. 3.6b by superimposing higher band $(1-2$ GHz) data over the lower $(0.5-1$ GHz).

Figure 3.6: Sample 1 - measured antenna impedance plot and transmission τ.

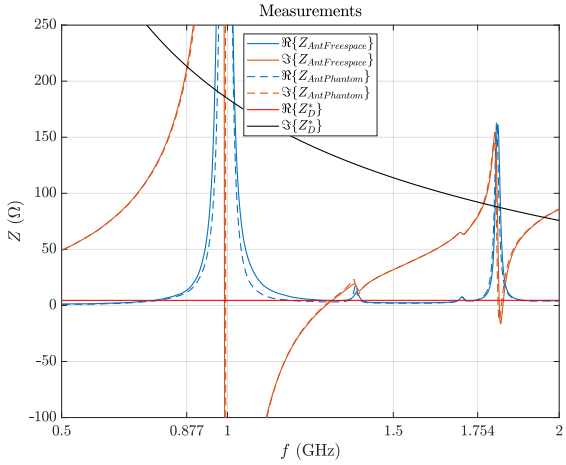

(a) : Measured antenna and simulated diode impedances.

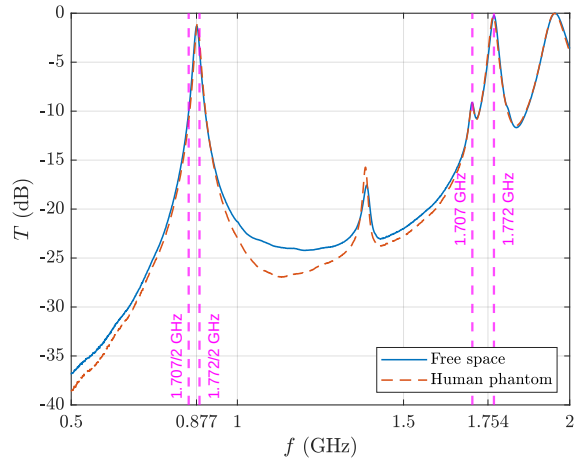

(b) : Transmission coefficient computed with (2.2).

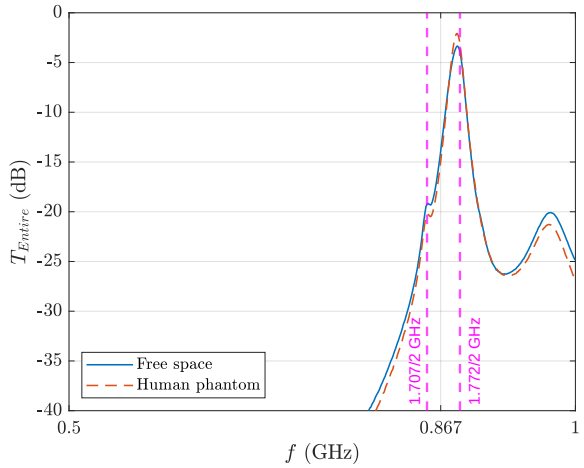

(c) : Combined transmission coefficient τ, computed from the data of Fig. 3.6b by superimposing higher band $(1-2$ GHz) data over the lower $(0.5-1$ GHz).

Figure 3.7: Sample 2 - measured antenna impedance plot and transmission τ.

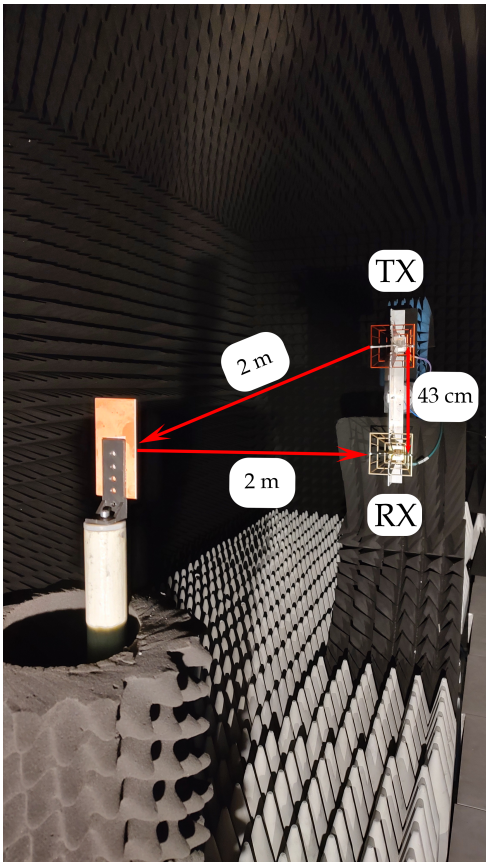

Figure 3.8: Measurement setup in an anechoic chamber. Tx and Rx antennas placed 43 cm away vertically from each other and both 2 m away from the tag.

3.4 Measurement of HT Conversion Loss and RSL

In this chapter, we show the measurement results of the RFID tag designed in chapter 2. The same equipment as listed in Table 3.1 was used. Two fabricated samples are shown in Fig. 3.9. The antenna was designed with a gap of 1 mm between the patch and the passive strips (Chapter 2), but a second sample with a gap of 2 mm was also fabricated to demonstrate the ability to encode data using FSC. A sample placed in an anechoic chamber is shown in Fig. 3.8. Setup details are annotated on the figure, such as the distances used to compute the Free Space Loss (FSL) for the estimation of CL.

More details regarding the measurement setup are shown in Fig. 3.10. frequency dependent gains and losses shown in the diagram are only approximate as their value depends on the frequency of operation. The power flow diagram gives an intuitive understanding on gains and losses in the system, thereby

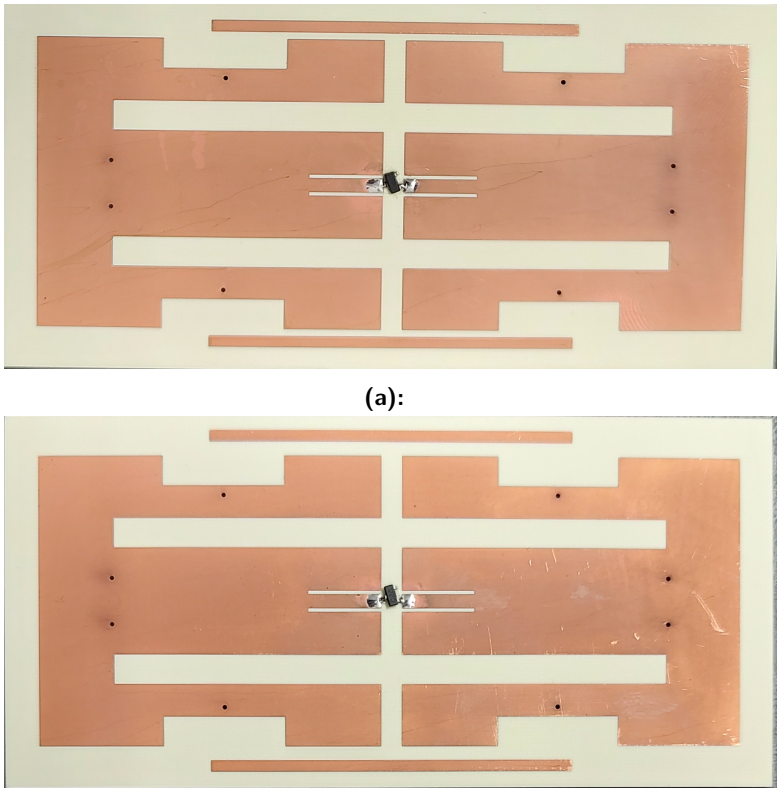

(a):

(b):

Figure 3.9: Fabricated RFID tag samples for testing with HSMS-2820 diode installed. The gap between the main antenna body and passive strips is: (a) 1 mm, and (b) 2 mm.

making it easy to estimate how much power is delivered to the transponder tag. Using the principle of power flow, both in uplink (tx) and downlink (rx), we computed power levels incident on the transponder, as well as, radiated by the transponder. This has allowed us to easily estimate CL of the transponder CL_{HT}. For the evaluation of CL_{HT}, we could use the power flow diagram shown in Fig. 3.10, and formulate the power incident on the transponder as following

$$P_{inc.} = P_{tx,\ 0.5\text{-}1\ GHz} + G_{tx,\ chain} + G_{att} + G_{tx,\ ant} + FSL_{2\ m,\ 0.5\text{-}1\ GHz} \quad (3.2)$$

where $P_{inc.}$ is the power incident on the transponder, $P_{tx,\ 0.5\text{-}1\ GHz}$ is the power output of the Vector Network Analyzer (VNA), $G_{tx,\ chain}$ is the tx chain gain (amplifier, Low Pass Filter (LPF), cables, attenuator (at 0 dB)), G_{att} is the gain of the attenuator that is varied from 0 dB to -50 dB in steps of -5 dB in order to obtain power sweep results, $G_{tx,\ ant}$ is the Tx antenna gain, and $FSL_{2\ m,\ 0.5\text{-}1\ GHz}$ is the FSL at 2 m in the range of 0.5 GHz to 1 GHz. All terms in (3.2) have units of dBm, dBi, or dB. Note that in the MATLAB code, all terms are column vectors of the same length except for

G_{att} having only 11 attenuation levels from 0 dB to −50 dB in steps of −5 dB. Also, $P_{tx,\ 0.5\text{-}1\ GHz}$ is simply a scalar 17 dBm since it is a constant output of the VNA. Also, note that all terms are defined as "gain", therefore in the uplink expression of (3.2), all terms are added whether it is gain or loss of the system.

Similarly, based on the power flow diagram in Fig. 3.10, we can define an expression for power radiated by the transponder as

$$P_{rad.} = P_{rx,\ 1\text{-}2\ GHz} - G_{rx,\ chain} - G_{rx,\ ant} - FSL_{2\ m,\ 1\text{-}2\ GHz} \tag{3.3}$$

where $P_{rad.}$ is the radiated power by the transponder, $P_{rx,\ 1\text{-}2\ GHz}$ is the received power by the VNA, $G_{rx,\ chain}$ is the Rx chain gain (losses due to cable from antenna to VNA), $G_{rx,\ ant}$ is the Rx antenna gain, and $FSL_{2\ m,\ 1\text{-}2\ GHz}$ is the free space loss vector at 2 m in the range of 1 GHz to 2 GHz. For clarity, the VNA in the experiment was configured to transmit in 0.5-1 GHz and receive in 1-2 GHz.

Having clearly defined $P_{inc.}$ and $P_{rad.}$ by expressions (3.2) and (3.3), we may simplify the power flow diagram as shown in Fig. 3.11 and arrive at the expression for CL_{HT}.

$$CL_{HT} = P_{inc.} - P_{rad.} \tag{3.4}$$

Obviously, $P_{rad.}$ is always less than $P_{inc.}$ because the transponder is passive, in other words, it does not generate its own power. With expression (3.4), we go ahead and evaluate conversion loss of both samples shown in Fig. 3.9. The resulting conversion losses were evaluated for different excitation powers and the figures are presented across the frequency of interest in Fig. 3.12. For completeness, the measured RSL for both samples is shown in Fig. 3.14. We must note that different excitation powers lead to different peaks in the measured received power due to changing impedance of the diode. Therefore, conversion loss also changes significantly revealing peaks at different frequencies as the excitation power is varied.

The RSL for both samples in Fig 3.14 demonstrates the FSC technique that was shown in S11 magnitude simulation earlier in Fig. 2.8. In simulation, the eight data identifiers were shown for different gaps between the patch and the passive strips varying from 0.9 mm to 1.4 mm. For the fabricated samples, in the RSL we have shown two distinguishable peaks in the vicinity of vertical pink lines of Fig 3.14. In this case, the difference between f_2 and $f_2 + \Delta f$ implements data identifier in accordance with simulated demonstration of Fig. 2.8. For an illustrative example, we have plotted one RSL data per each sample per excitation power in a single figure shown in Fig. 3.13, where peaks are clearly visible and whose parameters are summarized in Table 3.2.

Parameter	Sample 1 - value	Sample 2 - value
f_3	1.7488 GHz	1.7088 GHz
f_2	1.795 GHz	1.7869 GHz
$\|\Delta f\|$	46.2 MHz	78.1 MHz
$CL_{HT}\|_{f_3}$	29.2 dB	30.5 dB
$CL_{HT}\|_{f_2}$	5.7 dB	6.24 dB

Table 3.2: Measured parameters of the fabricated transponders.

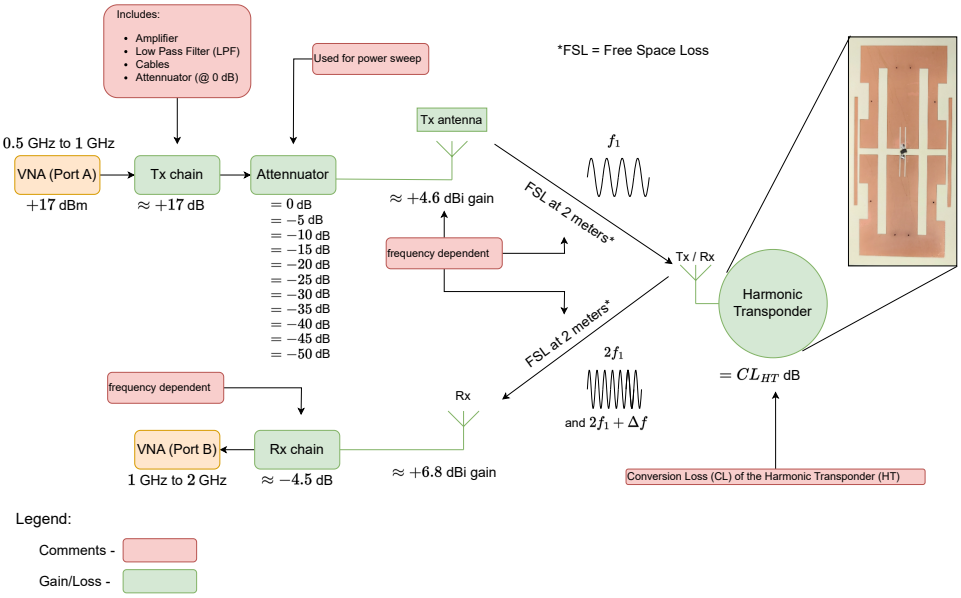

Figure 3.10: Power flow diagram in the measurement setup.

Note that these are not the best parameters as the CL as well as frequency detuning varies for different excitation powers. For a pair of frequencies in the RSL with better conversion loss (for the sample with 2 mm gap), the best conversion losses are 12.5 dB at 1.698 GHz and 10.7 dB at 1.768 GHz with the transmit power of approximately 17 dBm (see Fig. 3.12b).

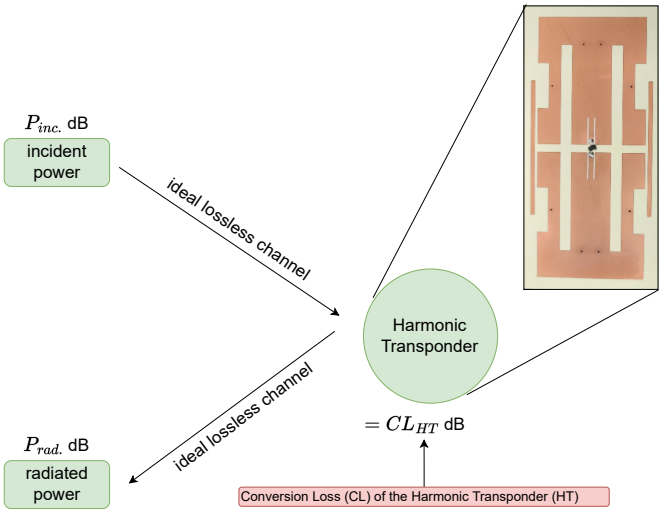

Figure 3.11: Simplified power flow diagram where all device gains and losses both in Tx and Rx chains are accounted for in $P_{inc.}$ and $P_{rad.}$ right up to the RFID tag.

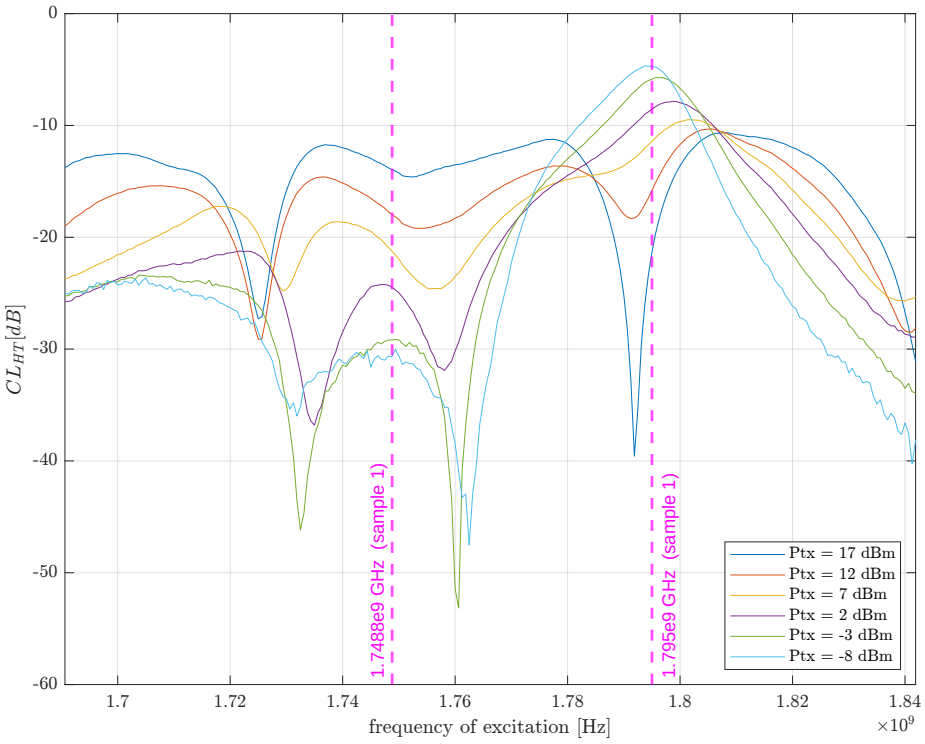

(a):

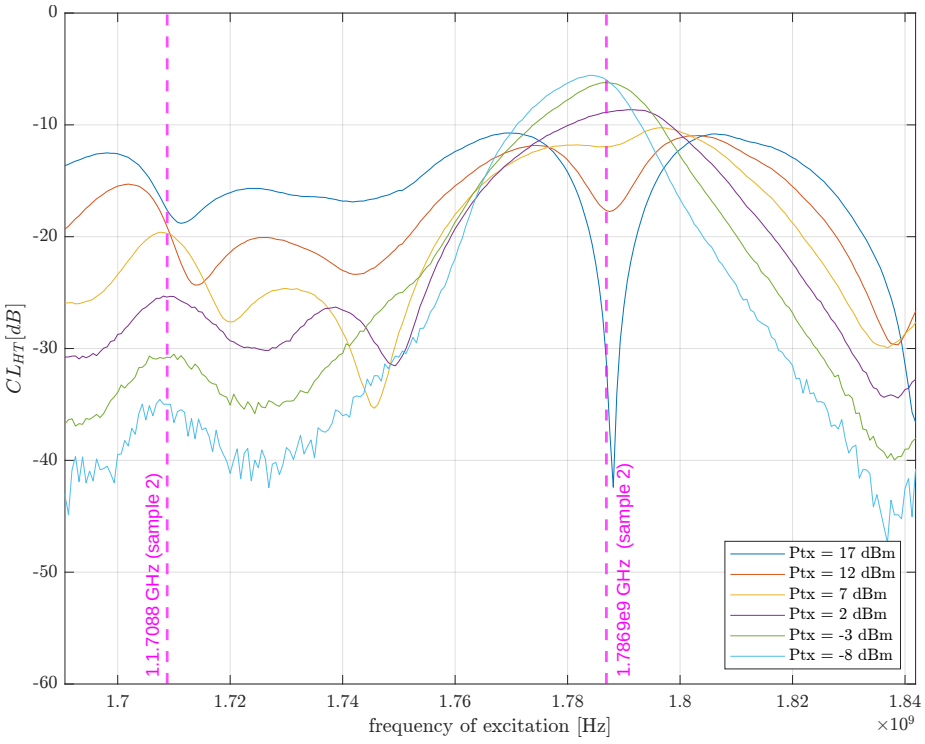

(b):

Figure 3.12: Conversion loss of the measured samples with different excitation powers for samples with (a) 1 mm gap and (b) 2 mm gap.

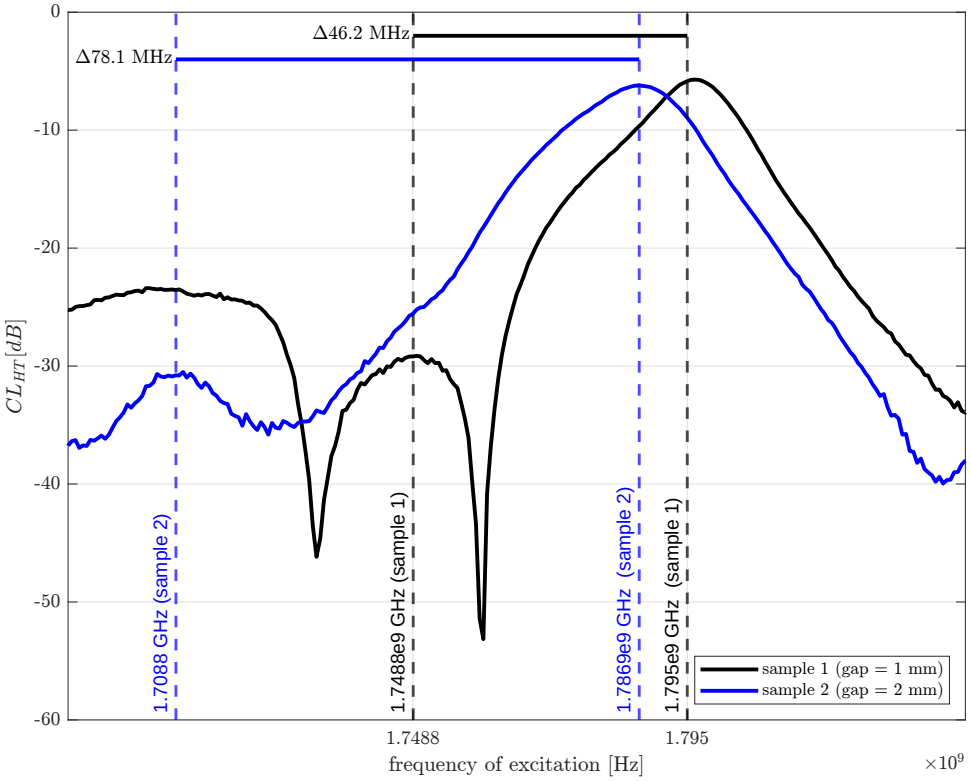

Figure 3.13: Conversion loss of the two samples with frequency shifts marked.

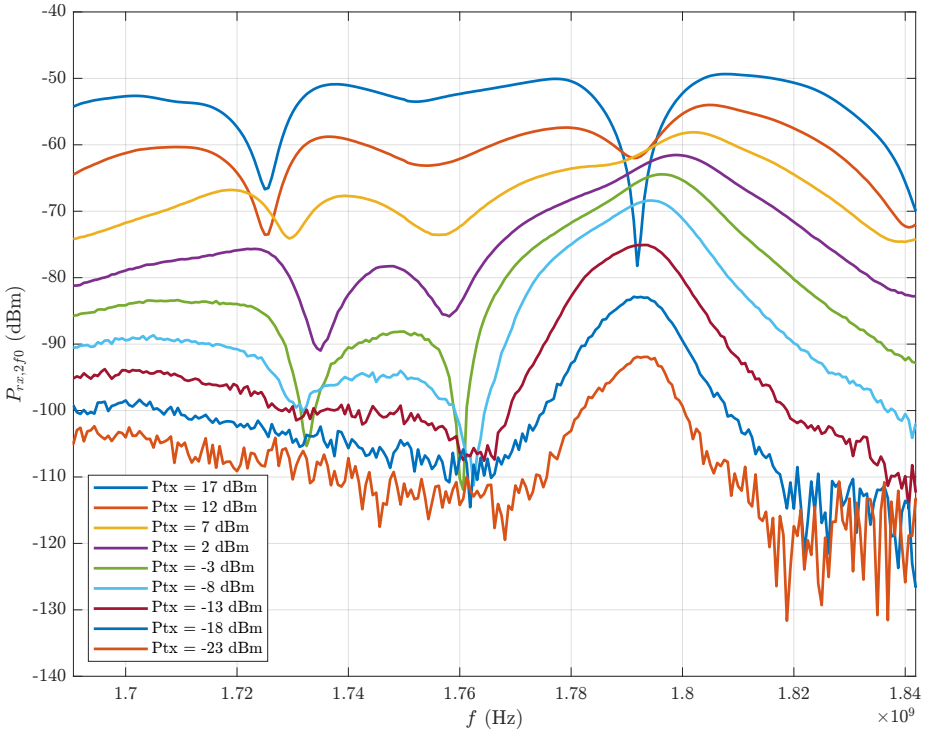

(a):

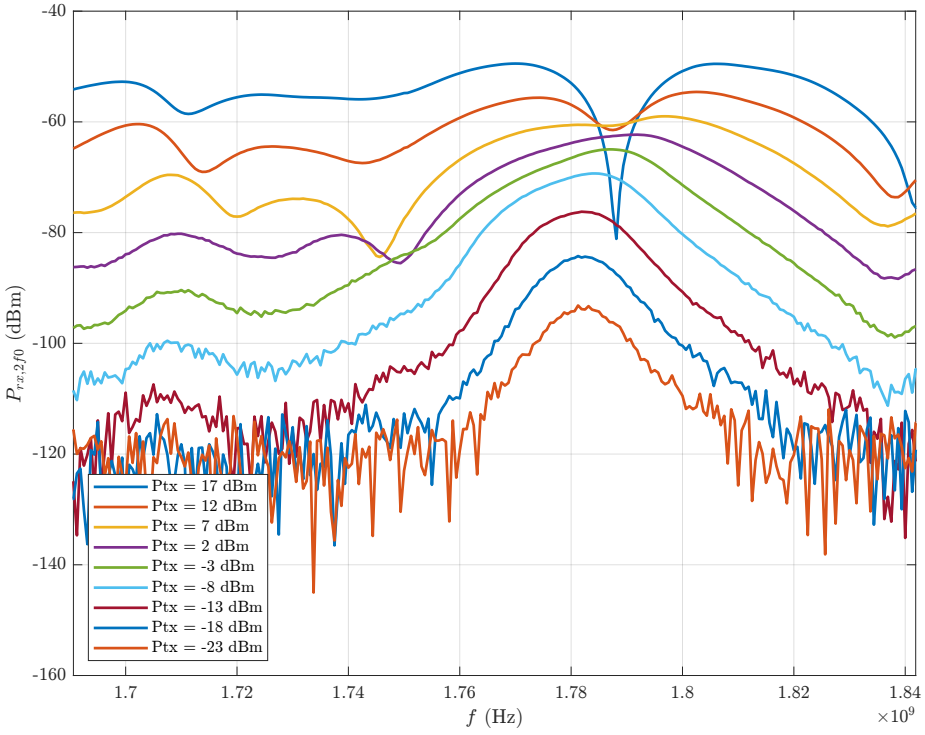

(b):

Figure 3.14: Measured received power for the samples with (a) 1 mm gap, and (b) 2 mm gap. The frequency spacing of the local peaks at frequencies f_2 and f_3 is used as an encoding mechanism to create a unique identifier of the HT (particularly visible in Fig. b) around $f_2 = 1.71$ GHz and $f_3 = 1.79$ GHz frequencies.

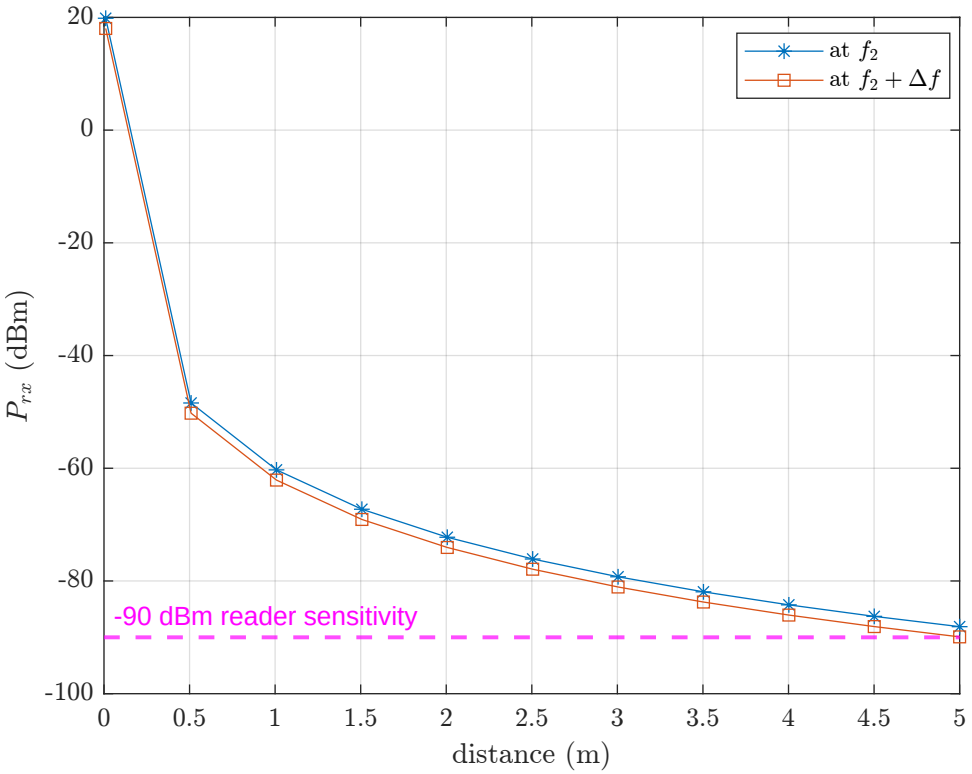

Figure 3.15: Reading distance estimation at f_2 and f_3.

3.5 Reading Distance

Based on the obtained data and known measurement setup parameters, it is possible to estimate reading distance of the proposed tag. The limiting factor in the reading distance is Equivalent Isotropically Radiated Power (EIRP), FSL, and the CL of the transponder at the frequencies where data is read. For the aforementioned analysis EIRP of 29 dBm and reader sensitivity of -90 dBm is assumed. Also, the best conversion losses have been used, i.e., 12.5 dB and 10.7 dB (obtained in the previous section). Results are shown in Fig. 3.15. As seen from the figure, reading distance is at least 5 meters, limited by the CL of the transponder and the EIRP.

Chapter 4

Conclusions and Further Work

In this thesis, an RFID-enabled harmonic transponder has been designed based on a triple-band patch-type antenna directly matched to a Schottky diode at three frequencies f_1, $2f_1$ and $2f_1 + \Delta f$. To implement the ID functionality, additional resonance was introduced at $2f_1 + \Delta f$ using a pair of passive strips gap-coupled to the patch antenna. To encode the data identifier on the transponder, the gap between the passive strips and the antenna patch was varied. Consequently, the data identifier was encoded as the frequency difference Δf between $2f_1$ and $2f_1 + \Delta f$. Simulation of the S11 parameter of the antenna showed that encoding at least eight data identifiers was possible. Samples based on simulation were fabricated and measured to verify the operation. It was revealed in the measured RSL that two distinct peaks appeared at expected frequencies with varying conversion losses depending on excitation power. Reading distance of about 5 meters was estimated in case of the EIRP of approximately 29 dBm with conversion losses of 12.5 dB and 10.7 dB.

A curious reader would have noticed that there is a fundamental limit to how much response can be captured at the receiver at the additional frequency ($2f_1 + \Delta f$) revealed by combined τ curves. This limit has to do with the finite "matching bandwidth" in the lower band of the transponder. By matching bandwidth we mean that around the fundamental design frequency $f_1 = 0.867\,\mathrm{GHz}$, the transmission coefficient is close to $0\,\mathrm{dB}$ (perfect transmission) only for a very narrow frequency range. This alone indicates that additional matched points in the higher band, which are not direct doubles of f_1, would show extremely low, though distinguishable, received power due to a sharp drop in the transmission coefficient in the lower band. This observation is also reflected in the evaluated conversion losses shown in

Table 3.2, where the additional resonances exhibit drastically worse conversion loss compared to that at the second harmonic.

This result is not surprising, since a previous work in [1] suggests that impedance matching at the fundamental is more important than at the second harmonic, based on the figure-of-merit expression derived by the author (raised to the power of 4 instead of squared). Considering the above limitation, for further work, increasing the bandwidth around f_1 or designing the antenna as quad-band may result in better transponder conversion loss at the second harmonic frequency and consequently in greater read range.

Appendix A

Diode impedance

For maximum power transfer between distributed networks, it is important to match their input impedances. In our case, the antenna's impedance must be matched to the diode's impedance at harmonically separated frequencies f_1 and $2f_1$. The matching would ensure that maximum power would be transferred to the diode at f_1 and maximum power would be utilized for creating the second harmonic at $2f_1$.

The antenna's impedance is extracted from CST Studio design suite after simulation. For the diode's impedance, we used a free SPICE simulator LTSpice to extract its frequency-dependent impedance. The technique of impedance extraction is quite simple and only requires using the diode manufacturer's provided SPICE model and correct IC package model.

The SPICE parameters of the HSMS-2820 diode are given in the datasheet provided by Avago Technologies [24]. The information on modelling SOT-23 and SOT-323 IC packages is given in Hewlett-Packard application note AN1124 [25].

From the LTSpice schematic provided with this work, the following steps must be taken to generate the correct file containing the complex frequency dependent impedance of the diode - *File > Export*. In the dialog window, *Z11(v_source)* must be selected for export. Also, *Polar: (dB,deg)* format must be selected. The given options for exporting are strongly recommended since the rest of the MATLAB code is prepared for this format of data. A user might want to regenerate the diode impedance from LTSpice as described above when the impedance matrix of particular frequency range and/or

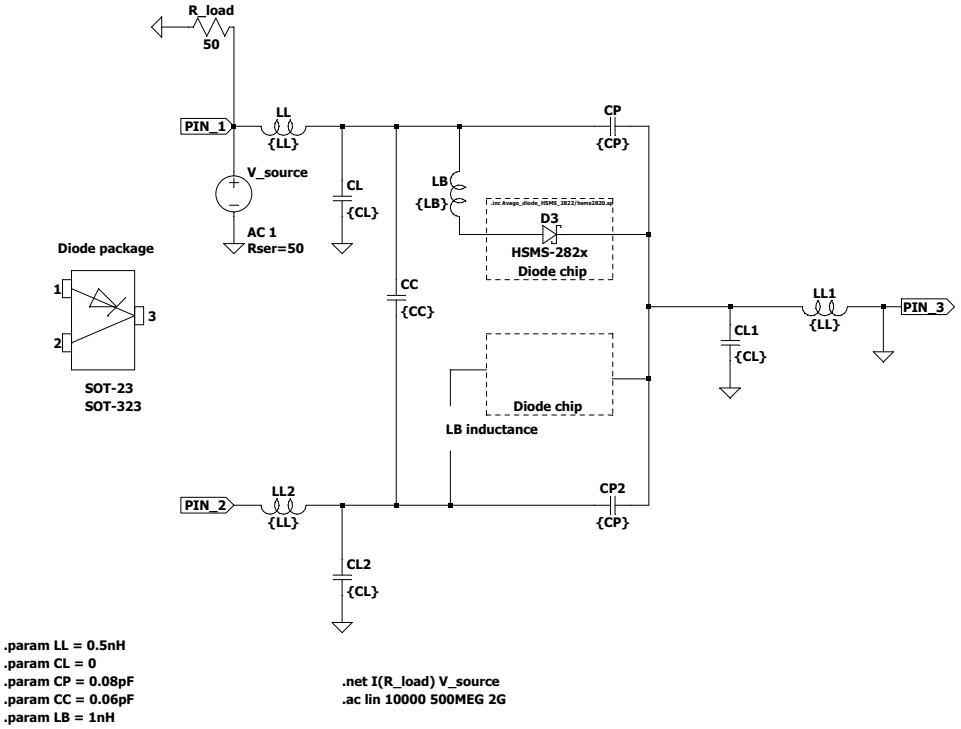

Figure A.1: Schematic from LTSpice simulator. SPICE parameters of the Schottky diode are included inside the HSMS-282x symbol (actual diode is HSMS-2820). The circuitry around the diode models the package. On the left is an illustrative top view of the IC.

number of data points is required. As shown at the bottom of Fig. A.1, the frequency range and the number of datapoints can be selected within the *.ac* SPICE command.

Appendix B

Bibliography

[1] K. Rasilainen, J. Ilvonen, A. Lehtovuori, J.-M. Hannula, and V. Viikari, "On design and evaluation of harmonic transponders," *IEEE Transactions on Antennas and Propagation*, vol. 63, no. 1, pp. 15–23, 2014.

[2] S. A. R. Parizi, "Bandwidth enhancement techniques," in *Microstrip Antennas: Trends in Research on*, vol. 1, BoD–Books on Demand, 2017.

[3] I. Jalaly and I. Robertson, "Rf barcodes using multiple frequency bands," in *IEEE MTT-S International Microwave Symposium Digest, 2005.*, pp. 139–142, IEEE, 2005.

[4] A. Vena, E. Perret, and S. Tedjini, "Chipless rfid tag using hybrid coding technique," *IEEE Transactions on Microwave Theory and Techniques*, vol. 59, no. 12, pp. 3356–3364, 2011.

[5] M. Polivka, V. Hubata-Vacek, and M. Svanda, "Harmonic balance/full-wave analysis of wearable harmonic transponder for iot applications," *IEEE Transactions on Antennas and Propagation*, vol. 70, no. 2, pp. 977–987, 2021.

[6] X. Qing, C. K. Goh, and Z. N. Chen, "Impedance characterization of rfid tag antennas and application in tag co-design," *IEEE Transactions on Microwave Theory and Techniques*, vol. 57, no. 5, pp. 1268–1274, 2009.

[7] K. Finkenzeller, *RFID handbook: fundamentals and applications in contactless smart cards, radio frequency identification and near-field communication*. John wiley & sons, 2010.

[8] A. N. Nambiar, "Rfid technology: A review of its applications," in *Proceedings of the world congress on engineering and computer science*,

vol. 2, pp. 20–22, International Association of Engineers Hong Kong, China, 2009.

[9] K. Rasilainen, J. Ilvonen, A. Lehtovuori, J.-M. Hannula, and V. Viikari, "Harmonic transponders: Performance and challenges," *Progress In Electromagnetics Research M*, vol. 41, pp. 139–147, 2015.

[10] K. Rasilainen and V. V. Viikari, "Transponder designs for harmonic radar applications," *International Journal of Antennas and Propagation*, vol. 2015, 2015.

[11] R. O. Hstger, "Harmonic radar systems for near-ground in-foliage nonlinear scatterers," *IEEE transactions on aerospace and electronic systems*, no. 2, pp. 230–245, 1976.

[12] H. A. Augenblick, "Dinade system as an anti-collision device," tech. rep., SAE Technical Paper, 1968.

[13] H. Kwun, G. L. Burkhardt, and J. L. Fisher, "Detection of reinforcing steel corrosion in concrete structures using non-linear harmonic and intermodulation wave generation," Jan. 19 1993. US Patent 5,180,969.

[14] J. Roland, G. McKinnon, C. Backhouse, and P. D. Taylor, "Even smaller radar tags on insects," May 1996.

[15] E. Cant, A. Smith, D. Reynolds, and J. Osborne, "Tracking butterfly flight paths across the landscape with harmonic radar," *Proceedings of the Royal Society B: Biological Sciences*, vol. 272, no. 1565, pp. 785–790, 2005.

[16] J. Riley and A. Smith, "Design considerations for an harmonic radar to investigate the flight of insects at low altitude," *Computers and Electronics in Agriculture*, vol. 35, no. 2-3, pp. 151–169, 2002.

[17] B. G. Colpitts and G. Boiteau, "Harmonic radar transceiver design: Miniature tags for insect tracking," *IEEE Transactions on Antennas and Propagation*, vol. 52, no. 11, pp. 2825–2832, 2004.

[18] G. Kumar and K. Gupta, "Broad-band microstrip antennas using additional resonators gap-coupled to the radiating edges," *IEEE Transactions on Antennas and Propagation*, vol. 32, no. 12, pp. 1375–1379, 1984.

[19] A. Vena, E. Perret, and S. Tedjini, "High-capacity chipless rfid tag insensitive to the polarization," *IEEE Transactions on Antennas and Propagation*, vol. 60, no. 10, pp. 4509–4515, 2012.

[20] M. Svanda, M. Polivka, J. Havlicek, J. Machac, and D. H. Werner, "Platform tolerant, high encoding capacity dipole array-plate chipless rfid tags," *IEEE Access*, vol. 7, pp. 138707–138720, 2019.

[21] B. Razavi and R. Behzad, *RF microelectronics*, vol. 2. Prentice hall New York, 2012.

[22] V. Hubata-Vacek, "Dvoupásmová vázaná mikropásková anténa jako harmonickỳ transpondér pro činnost na lidském těle," Master's thesis, České vysoké učení technické v Praze. Vypočetní a informační centrum., 2020.

[23] M. Polivka and J. Frolik, "On performance metrics for harmonic transponders," *IEEE Transactions on Antennas and Propagation*, 2023.

[24] "HSMS-282x Surface Mount RF Schottky Barrier Diodes." `https://eu.mouser.com/datasheet/2/678/avagotechnologies_AV02-1320EN,0-1217119.pdf`. Accessed: 2023-05-18.

[25] "AN1124 - Linear Models for Diode Surface Mount Packages." `http://www.hp.woodshot.com/hprfhelp/4_downld/lit/diodelit/an1124.pdf`. Accessed: 2023-05-21.